Large-scale stability and astronomical constraints for coupled dark-energy models

Weiqiang Yang,[1,*] Supriya Pan,[2,3,†] and John D. Barrow[4,‡]

[1]Department of Physics, Liaoning Normal University, Dalian 116029, People's Republic of China
[2]Department of Physical Sciences, Indian Institute of Science Education and Research, Kolkata, Mohanpur, West Bengal 741246, India
[3]Department of Mathematics, Raiganj Surendranath Mahavidyalaya, Sudarshanpur, Raiganj, West Bengal 733134, India
[4]DAMTP, Centre for Mathematical Sciences, University of Cambridge, Wilberforce Road, Cambridge CB3 0WA, United Kingdom

(Received 15 June 2017; published 26 February 2018)

We study large-scale inhomogeneous perturbations and instabilities of interacting dark-energy models. Past analysis of large-scale perturbative instabilities has shown that we can only test interacting dark-energy models with observational data when their parameter ranges are either $w_x \geq -1$ and $\xi \geq 0$, or $w_x \leq -1$ and $\xi \leq 0$, where w_x is the dark-energy equation of state and ξ is a coupling parameter governing the strength and direction of the energy transfer. We show that by adding a factor $(1 + w_x)$ to the background energy transfer, the whole parameter space can be tested against all the data, and thus, the instabilities in such interaction models can be removed. We test three classes of interaction models using the latest astronomical data from the CMB, supernovae, baryon acoustic oscillations, redshift-space distortions, weak lensing, cosmic chronometers, and the local Hubble constant. Precise constraints are found. Our analysis shows that a very small but nonzero deviation from pure Λ-cosmology is suggested by the observational data, while the no-interaction scenario can be recovered at the 68.3% confidence level. In particular, for three interacting dark-energy (IDE) models, identified as IDE 1, IDE 2, and IDE 3, the 68.3% confidence-level constraints on the interaction coupling strengths are $\xi = 0.0360^{+0.0091}_{-0.0360}$ (IDE 1), $\xi = 0.0433^{+0.0062}_{-0.0433}$ (IDE 2), $\xi = 0.1064^{+0.0437}_{-0.1064}$ (IDE 3). In addition, we find that the dark-energy equation of state tends towards the phantom region. Taking the 68.3% confidence-level constraints, $w_x = -1.0230^{+0.0329}_{-0.0257}$ (IDE 1), $w_x = -1.0247^{+0.0289}_{-0.0302}$ (IDE 2), and $w_x = -1.0275^{+0.0228}_{-0.0318}$ (IDE 3). However, the possibility of $w_x > -1$ is also not rejected by the astronomical data employed in this analysis. Moreover, we find in all interaction models that, as the value of the Hubble constant decreases, the behavior of the dark-energy equation of state shifts from a phantom to a quintessence type with its equation of state very close to that of a simple cosmological constant at the present time. Finally, we compare the observational estimations of the coupling strength imposed on some interaction models studied in this work with the past constraints obtained on them for different regions of the dark-energy equation of state.

DOI: 10.1103/PhysRevD.97.043529

I. INTRODUCTION

The physics of dark energy (DE) and dark matter is still an open issue in cosmology. Dark energy occupies about 68.5% of the total energy density of the Universe today [1] and is believed to accelerate its observed expansion, but the physical nature, origin, and time evolution of this dark energy remain unknown. On the other hand, the dark-matter sector (occupying almost 27.5% of the total energy density of the present-day Universe) appears to be the principal gravitational influence on the formation of large-scale structure in the Universe, and its existence is supported by direct evidence from the spiral galaxy rotation curves and cluster dynamics [2]. At present, we have many dark-energy models [3,4] and, according to syntheses of all the current observational data, Λ-cosmology appears to be the simplest cosmological model that can explain the bulk of the evidence. However, the unexplained numerical value of the cosmological constant, and the coincidences between the present densities of the different dark and luminous components of the Universe, provoke us to search for new cosmological scenarios in which the observed state of affairs is more natural. In this work, we explore cosmologies where dark energy interacts and exchanges energy with dark matter.

*d11102004@163.com
†span@research.jdvu.ac.in
‡jdb34@damtp.cam.ac.uk

Originally, the possibility that dark energy might interact with dark matter was introduced to justify the very small value of the cosmological constant by Wetterich [5,6]. However, when dynamical models were introduced as alternatives to a simple (noninteracting) cosmological constant, it was found that interactions between dark energy and dark matter might provide a simple explanation for the cosmic coincidence problem [7]. If one views this interaction from the particle physics perspective, then it is natural that the two fields should interact with each other nongravitationally [8]. Models of this type are known as interacting, or coupled, dark-energy models.

The interacting dynamics is described by a new function Q, which determines the form of the coupling between dark matter and dark energy via their conservation equations as $\nabla_\nu T_c^{\mu\nu} = -Q$ and $\nabla_\nu T_x^{\mu\nu} = Q$, where $T_c^{\mu\nu}$ and $T_x^{\mu\nu}$ are, respectively, identified as the energy-momentum tensors for cold dark matter (CDM) and DE. Consequently, one can further identify ρ_c and ρ_x to be the energy densities of CDM and DE fluids, respectively. Until now, there have been many interacting dark-energy models based on different proposals for the form of energy exchange term Q. A series of investigations have been performed using observational data with interesting results [9–35]. Aside from the specific issue of dark-matter–dark-energy interactions, we can also view the interaction Q as an energy exchange between any two barotropic fluids (see Ref. [36]).

The interacting fluid models are generally well behaved when one only considers their effects on the background evolution. However, the analysis of inhomogeneous cosmological perturbations is essential to provide a fuller picture of these models, to determine if they are stable or unstable components of the large-scale structure of the Universe. For example, a simple energy exchange term $Q \propto \rho_c$ leads to an instability in the dark-matter perturbations at early times since the curvature perturbation blows up on super-Hubble scales [27]. In order to derive a stable perturbation evolution, another simple interaction term, $Q \propto \rho_x$, needs to be tested by the observations with two intervals of possible dark-energy equations of state: $w_x \leq -1$ and $w_x \geq -1$ [29–33]. Therefore, the principal motivation of this paper is to find a form of energy transfer Q that could alleviate the perturbative instability. In this way, we might test the full parameter space of dark-energy equations of state by the observations, allowing for even the possibility of a "phantom" equation of state. In this respect, large-scale structure information, such as redshift-space distortion (RSD) [37–40] and weak gravitational lensing [41–43], provides an important tools to break any degeneracy of cosmological models. This view has already been confirmed by many investigations [44–53]. One conclusion from these studies was that joint measurements of the geometry and dynamical observations found that the interaction rate Q was zero at about 1σ [30–33]. Unfortunately, this conclusion has been drawn using the intervals $w_x \leq -1$ and $w_x \geq -1$ separately. If we could test the interacting dark-energy model with the full parameter space of w_x against the observations, then a different conclusion might be found, which is one aim of this paper.

The paper is outlined as follows. In Sec. II, we describe the perturbation equations for the interacting dark-energy models. Section III contains a brief description of the observational data used in our analysis. In Sec. IV, we discuss the main observational results extracted from the interacting models in our study. Finally, in Sec. V, we conclude with a short summary.

II. BACKGROUND AND PERTURBATION EVOLUTION IN COUPLED DARK-ENERGY MODELS

In this section we describe the dynamics of the coupled dark-energy model at both the background and perturbative levels. As usual, we consider a spatially flat Friedmann-Lemaître-Robertson-Walker (FLRW) universe characterized by the metric line element

$$ds^2 = -dt^2 + a^2(t)[dr^2 + r^2(d\theta^2 + \sin^2\theta d\phi^2)],$$

where $a(t)$ is the expansion scale factor and t is the comoving proper time. The total energy density of the Universe is $\rho_t = \rho_c + \rho_x + \rho_b + \rho_r$, where we identify each ρ_i as the energy density of the ith fluid component (the subscripts c, x, b, and r, respectively, stand for cold dark matter, dark energy, baryons, and radiation). The cold dark matter is pressureless, and we assume the dark energy is barotropic. In order to neglect any kind of inflexible constraints like a "fifth force," we assume that the baryons and radiation are conserved separately; in other words, they follow the usual conservation laws without any interaction. Now, in such a spacetime, the modified conservation equations for cold dark matter and dark energy are assumed to have the following forms,

$$\rho_c' + 3\mathcal{H}\rho_c = -aQ, \tag{1}$$

$$\rho_x' + 3\mathcal{H}(1 + w_x)\rho_x = aQ, \tag{2}$$

where a prime $'$ denotes differentiation with respect to the conformal time, $\mathcal{H} = a'/a$ is the conformal Hubble parameter, and w_x is the equation-of-state parameter of dark energy. The positive energy exchange term shows that the energy transfer is from dark matter to dark energy, and negative Q denotes the opposite case. Further, one can see that the conservation equations (1) and (2) can be rewritten by introducing effective equations of state for the dark fluids as

$$\rho_c' + 3\mathcal{H}(1 + w_c^{\text{eff}})\rho_c = 0,$$
$$\rho_x' + 3\mathcal{H}(1 + w_x^{\text{eff}})\rho_x = 0,$$

where $w_c^{\rm eff}$, $w_x^{\rm eff}$ are defined as the effective equation-of-state parameters for CDM and dark energy with

$$w_c^{\rm eff} = \frac{aQ}{3\mathcal{H}\rho_c}, \qquad w_x^{\rm eff} = w_x - \frac{aQ}{3\mathcal{H}\rho_x}.$$

We note that the effective equation-of-state parameter for CDM could be nonzero, while the effective equation of state for dark energy offers several possibilities depending on the strength of the interaction rate Q. In particular, the direction of energy transfer controls the nature of an effective dark energy ("phantom" or "quintessence" or an "equivalent cosmological constant" scenario) fluid through the quantity $w_x^{\rm eff}$. Finally, the Friedmann equation is

$$\mathcal{H}^2 = \frac{8\pi G}{3} a^2(\rho_c + \rho_x + \rho_b + \rho_r),$$

which constrains the dynamics of the Universe. Thus, the system of Eqs. (1) and (2), together with the Friedmann equation, determines the entire dynamics of the Universe, once the energy transfer rate Q is specified.

We now discuss the linear perturbations for the interacting models that we introduce here. The metric that determines the most general scalar mode perturbation is given by [54–56]

$$ds^2 = a^2(\tau)[-(1+2\phi)d\tau^2 + 2\partial_i B d\tau dx^i + ((1-2\psi)\delta_{ij} + 2\partial_i\partial_j E)dx^i dx^j],$$

where the quantities ϕ, B, ψ, and E, respectively, stand for the gauge-dependent scalar perturbations, and τ is the conformal time. Now, for any fluid subscripted by "A," its energy-momentum conservation equations can be calculated and are [27–29]

$$\nabla_\nu T_A^{\mu\nu} = Q_A^\mu, \qquad \sum_{\rm A} Q_A^\mu = 0,$$

where one has $Q_A^\mu = (Q_A + \delta Q_A)u^\mu + a^{-1}(0, \partial^i f_A)$ relative to the four-velocity u^μ [27–29]. We specialize the momentum transfer potential to be the simplest physical choice, which is zero in the rest frame of dark matter [27,29,57]. Hence, the momentum transfer potential becomes $k^2 f_A = Q_A(\theta - \theta_c)$. We define the pressure perturbation by $\delta p_A = c_{sA}^2\delta\rho_A + (c_{sA}^2 - c_{aA}^2)\rho_A'(v_A + B)$ [27,58,59], where $c_{aA}^2 = p_A'/\rho_A' = w_x + w_x'/(\rho_A'/\rho_A)$ is the physical sound speed of the fluid A in the rest frame. If we further define the density contrast by $\delta_A = \delta\rho_A/\rho_A$ and consider $\pi_A = 0$, then in the synchronous gauge, equivalently, $\phi = B = 0$, $\psi = \eta$, and $k^2 E = -h/2 - 3\eta$, the general evolution equations for the density perturbation (i.e., the continuity equation) and the velocity perturbation (Euler equation) equations for dark energy and dark matter, respectively, become

$$\delta_x' = -(1+w_x)\left(\theta_x + \frac{h'}{2}\right) - 3\mathcal{H}(c_{sx}^2 - w_x)\left[\delta_x + 3\mathcal{H}(1+w_x)\frac{\theta_x}{k^2}\right] - 3\mathcal{H}w_x'\frac{\theta_x}{k^2} + \frac{aQ}{\rho_x}\left[-\delta_x + \frac{\delta Q}{Q} + 3\mathcal{H}(c_{sx}^2 - w_x)\frac{\theta_x}{k^2}\right], \tag{3}$$

$$\theta_x' = -\mathcal{H}(1 - 3c_{sx}^2)\theta_x + \frac{c_{sx}^2}{(1+w_x)}k^2\delta_x + \frac{aQ}{\rho_x}\left[\frac{\theta_c - (1+c_{sx}^2)\theta_x}{1+w_x}\right], \tag{4}$$

$$\delta_c' = -\left(\theta_c + \frac{h'}{2}\right) + \frac{aQ}{\rho_c}\left(\delta_c - \frac{\delta Q}{Q}\right), \tag{5}$$

$$\theta_c' = -\mathcal{H}\theta_c, \tag{6}$$

where the term $\delta Q/Q$ includes the perturbation term for the Hubble expansion rate, δH (we note that $\mathcal{H} = aH$). From the perturbation of the Hubble expansion rate, δH, one could obtain the gauge-invariant equations for the coupled dark sector [60]. Thus, we consider the perturbation of the Hubble expansion rate since the total expansion rate would include two parts: background and perturbation. In the light of the analysis of the contribution from the perturbation of the expansion rate in Ref. [60], it is chosen to be associated with the volume expansion of the total fluid, i.e., $\delta H/H = (\theta + h'/2)/(3\mathcal{H})$.

The energy transfer may change the history of the Universe. In most of the cases, interacting models are reliable when their background evolution is considered. However, it is also very important to take care of the cosmological perturbations in order to ensure the stability of the cosmological models under consideration. The Hubble rate is assumed to be the average expansion rate in Q. One should treat H as a local variable so as to include the perturbation term δH. Thus, we can consistently obtain the gauge-invariant perturbation equations [61].

In the following, we discuss the stability and instability issues associated with the current interacting models. The large-scale instability arises from the pressure perturbation of dark energy [27]. The pressure perturbation includes the adiabatic pressure perturbation and the intrinsic nonadiabatic pressure perturbation. For the interacting dark-energy models, the nonadiabatic part might grow fast at early times due to the energy transfer, and this leads to rapid growth of the curvature perturbation on large scales. For example, as mentioned above, the simple energy exchange term $Q \propto \rho_c$ leads to an instability in the dark-matter perturbations at early times since the curvature perturbation blows up on super-Hubble scales [27]. Subsequently, another interaction model $Q = 3H\xi\rho_c\rho_x/(\rho_c + \rho_x)$ was suggested in Ref. [62], where it was shown that this form of Q for the energy

transfer could avoid the large-scale instability during the early expansion of the Universe.

The pressure perturbation for the coupled dark-energy models is given by [58,60]

$$\begin{aligned}\delta p_x &= c_{sx}^2\delta\rho_x - (c_{sx}^2 - c_{ax}^2)\rho_x'\frac{\theta_x}{k^2},\\ &= c_{sx}^2\delta\rho_x + 3\mathcal{H}\rho_x(1+w_x)(c_{sx}^2 - c_{ax}^2)\\ &\quad\times\left[1 - \frac{aQ}{3\mathcal{H}\rho_x(1+w_x)}\right]\frac{\theta_x}{k^2},\\ &= c_{sx}^2\delta\rho_x + 3\mathcal{H}\rho_x(1+w_x)(c_{sx}^2 - c_{ax}^2)(1+d)\frac{\theta_x}{k^2}. \quad (7)\end{aligned}$$

Now, one could judge the stability condition of the perturbations via the "doom factor" [60], defined as

$$d \equiv -aQ/[3\mathcal{H}\rho_x(1+w_x)],$$

using the pressure perturbation of dark energy. Thus, stability can be realized when $d \leq 0$ [29,60]. It means that for the usual interaction rates in the literature, $Q = 3H\xi\bar{Q}$ (with $\bar{Q} > 0$), the perturbation stability requires the conditions $\xi \geq 0$ and $(1+w_x) > 0$ or $\xi \leq 0$ and $(1+w_x) < 0$. Following this, the interaction term $Q = 3H\xi\rho_x$ needs to be tested against the observations with two intervals for the dark-energy equation of state, $w_x \leq -1$ and $w_x \geq -1$ [29–33]. We note that $w_x = -1$ is the limiting case (see [29] for details). Now, looking at the pressure perturbations in Eq. (7), it is worth noting that the interaction functions with $(1+w_x)$ could release the prior of the DE equation of state, which is a very interesting property because the prior on the dark-energy equation of state plays a crucial role in the statistical analysis. Thus, here we assume a phenomenological energy transfer which includes the factor $(1+w_x)$ explicitly—for example, of the form $Q = 3H\xi(1+w_x)\rho_x$, $Q = 3H\xi(1+w_x)\rho_c\rho_x/(\rho_c+\rho_x)$, $Q = 3H\xi(1+w_x)\rho_x^\alpha\rho_c^\beta$, or the general form $Q = 3H\xi(1+w_x)\rho_c^\alpha\rho_x^\gamma(\rho_c+\rho_x)^\beta$, where w_x might be constant or time dependent. Thus, we can define the doom factor for the coupled model

$$d \equiv -\frac{aQ}{3\mathcal{H}\rho_x(1+w_x)} = -\xi\rho_c^\alpha\rho_x^{\gamma-1}(\rho_c+\rho_x)^\beta.$$

Now, it is easy to see that in order to have the stable perturbations, i.e., $d \leq 0$, the coupling parameter should satisfy the relation $\xi \geq 0$. That means there is no need to test the interaction models for two intervals of the dark-energy equation of state, namely, $w_x \leq -1$ and $w_x \geq -1$ [30–33]; rather, we could just constrain the full parameter space of w_x using the observational data. Thus, with the simple constraint on the coupling parameter that $\xi \geq 0$, we can alleviate the large-scale perturbation instabilities in the coupled dark-energy models—this is the novelty of the present work. In this way, we can explore the possibility of a phantom dark-energy equation of state. It should be noted that, for some suitable time-varying dark-energy equations of state, such as the Chevallier-Polarski and Linder (CPL) parametrization [63,64], the perturbation instability could also be alleviated [28]. However, we note that the proposed general interaction model $Q = 3H\xi(1+w_x)\rho_c^\alpha\rho_x^\gamma(\rho_c+\rho_x)^\beta$ can be viewed as $Q = 3H\bar{\xi}\rho_c^\alpha\rho_x^\gamma(\rho_c+\rho_x)^\beta$ using a simple transformation $\xi \to \bar{\xi} = \xi(1+w_x)$. Now, we observe that, if one allows the dark-energy equation of state to run beyond the cosmological constant limit, i.e., $w_x \leq -1$, then considering the stability condition $d \leq 0$, the model could produce stable perturbations on large scales for $\bar{\xi} \leq 0$. This is an alternative route to produce the stable perturbations from interaction models for the large-scale structure of the Universe [29–33] without introducing the factor $(1+w_x)$ explicitly outside the interaction rate.

Next, we recall the general interaction model which recovers the three interactions used in our study above. Since this general interaction assumes the expression

$$Q = 3H\xi(1+w_x)\rho_c^\alpha\rho_x^\gamma(\rho_c+\rho_x)^\beta,$$

where the exponents $(\alpha,\beta,\gamma) \in \mathbb{R}^3$ must satisfy $\alpha+\beta+\gamma = 1$, so that the dimension of Q is in accordance with the background energy-momentum conservation equation, then, using the relation $\gamma = 1-\alpha-\beta$, we may rewrite Q as $Q = 3H\xi(1+w_x)\rho_c^\alpha\rho_x^{1-\alpha-\beta}(\rho_c+\rho_x)^\beta$. Now, for this interaction the variation δQ reads

$$\delta Q = Q\left[\alpha\delta_c + (1-\alpha-\beta)\delta_x + \beta\frac{\rho_c\delta_c+\rho_x\delta_x}{\rho_c+\rho_x} + \frac{\theta+h'/2}{3\mathcal{H}}\right],$$

and consequently, the density and velocity perturbation equations for dark energy and dark matter for this Q become

$$\begin{aligned}\delta_x' &= -(1+w_x)\left(\theta_x + \frac{h'}{2}\right) - 3\mathcal{H}(c_{sx}^2 - w_x)\left[\delta_x + 3\mathcal{H}(1+w_x)\frac{\theta_x}{k^2}\right] - 3\mathcal{H}w_x'\frac{\theta_x}{k^2}\\ &\quad + 3\mathcal{H}\xi(1+w_x)\rho_c^\alpha\rho_x^{-\alpha-\beta}(\rho_c+\rho_x)^\beta\left[\alpha\delta_c - (\alpha+\beta)\delta_x + \beta\frac{\rho_c\delta_c+\rho_x\delta_x}{\rho_c+\rho_x} + \frac{\theta+h'/2}{3\mathcal{H}} + 3\mathcal{H}(c_{sx}^2 - w_x)\frac{\theta_x}{k^2}\right], \quad (8)\end{aligned}$$

$$\theta_x' = -\mathcal{H}(1-3c_{sx}^2)\theta_x + \frac{c_{sx}^2}{(1+w_x)}k^2\delta_x + 3\mathcal{H}\xi\rho_c^\alpha\rho_x^{-\alpha-\beta}(\rho_c+\rho_x)^\beta[\theta_c - (1+c_{sx}^2)\theta_x], \quad (9)$$

$$\delta_c' = -\left(\theta_c + \frac{h'}{2}\right) + 3\mathcal{H}\xi(1+w_x)\rho_c^{\alpha-1}\rho_x^{1-\alpha-\beta}(\rho_c+\rho_x)^{\beta} \times \left[(1-\alpha)\delta_c - (1-\alpha-\beta)\delta_x - \beta\frac{\rho_c\delta_c+\rho_x\delta_x}{\rho_c+\rho_x} - \frac{\theta+h'/2}{3\mathcal{H}}\right], \quad (10)$$

$$\theta_c' = -\mathcal{H}\theta_c, \quad (11)$$

where $\alpha \leq 0$ or $\beta \leq 0$ is required for the perturbation evolution to be stable at early times, according to the analysis of large-scale instability [27]. These perturbation equations of dark energy and dark matter include many coupled dark-energy models. For example, if $\beta = 0$, the stability requirement $\alpha \leq 0$ favors the coupling $Q = 3H\xi(1+w_x)\rho_c^{\alpha}\rho_x^{1-\alpha}$. For $\alpha = -1$ and $\beta = 0$, we get the coupling $Q = 3H\xi(1+w_x)\rho_x^2/\rho_c$. When $\alpha = 1$ and $\beta = -1$, we have $Q = 3H\xi(1+w_x)\rho_c\rho_x/(\rho_c+\rho_x)$. Further, for $\alpha = \beta = 0$, we could obtain the simplest energy transfer, with $Q = 3H\xi(1+w_x)\rho_x$. We note that the explicit appearance of the Hubble factor H in the interaction function is, in general, not necessary in spatially flat universes. However, its appearance helps us write the conservation equations with respect to the lapse function or the scale factor of the FLRW universe.[1] Moreover, the volume factor "3" has no physical meaning; this is just for simplicity without any loss of generality. We note that the perturbation equations are valid when the dark-energy equation of state is time dependent, such as CPL [63,64]. Now, for some particular choices of α, β, we test three interacting dark-energy models against the observational data sets when the dark-energy equation of state is assumed to be constant.

We consider first the simplest interacting dark-energy model (labeled IDE 1), with $\alpha = 0$ and $\beta = 0$. The coupling Q thus becomes

$$Q = 3H\xi(1+w_x)\rho_x.$$

For this model, following [61], we calculate that $\delta Q = Q[\delta_x + (\theta + h'/2)/(3\mathcal{H})]$. Thus, the perturbation equations for dark energy and dark matter become

$$\delta_x' = -(1+w_x)\left(\theta_x + \frac{h'}{2}\right) - 3\mathcal{H}(c_{sx}^2 - w_x)\left[\delta_x + 3\mathcal{H}(1+w_x)\frac{\theta_x}{k^2}\right] + 3\mathcal{H}\xi(1+w_x)\left[\frac{\theta+h'/2}{3\mathcal{H}} + 3\mathcal{H}(c_{sx}^2 - w_x)\frac{\theta_x}{k^2}\right], \quad (12)$$

$$\theta_x' = -\mathcal{H}(1-3c_{sx}^2)\theta_x + \frac{c_{sx}^2}{(1+w_x)}k^2\delta_x + 3\mathcal{H}\xi[\theta_c - (1+c_{sx}^2)\theta_x], \quad (13)$$

$$\delta_c' = -\left(\theta_c + \frac{h'}{2}\right) + 3\mathcal{H}\xi(1+w_x)\frac{\rho_x}{\rho_c}\left(\delta_c - \delta_x - \frac{\theta+h'/2}{3\mathcal{H}}\right), \quad (14)$$

$$\theta_c' = -\mathcal{H}\theta_c. \quad (15)$$

Next we consider the second interaction model (IDE 2) for the specific values of the parameters $\alpha = 1$ and $\beta = -1$. The coupling for such a choice becomes

$$Q = 3H\xi(1+w_x)\frac{\rho_c\rho_x}{(\rho_c+\rho_x)}.$$

Consequently, we have $\delta Q = Q[\delta_c + \delta_x - (\rho_c\delta_c + \rho_x\delta_x)/(\rho_c+\rho_x) + (\theta + h'/2)/(3\mathcal{H})]$, and similarly the perturbation equations of dark energy and dark matter follow:

$$\delta_x' = -(1+w_x)\left(\theta_x + \frac{h'}{2}\right) - 3\mathcal{H}(c_{sx}^2 - w_x)\left[\delta_x + 3\mathcal{H}(1+w_x)\frac{\theta_x}{k^2}\right] + 3\mathcal{H}\xi(1+w_x)\frac{\rho_c}{\rho_c+\rho_x}\left[\delta_c - \frac{\rho_c\delta_c+\rho_x\delta_x}{\rho_c+\rho_x} + \frac{\theta+h'/2}{3\mathcal{H}} + 3\mathcal{H}(c_{sx}^2 - w_x)\frac{\theta_x}{k^2}\right], \quad (16)$$

$$\theta_x' = -\mathcal{H}(1-3c_{sx}^2)\theta_x + \frac{c_{sx}^2}{(1+w_x)}k^2\delta_x + 3\mathcal{H}\xi\frac{\rho_c}{\rho_c+\rho_x}[\theta_c - (1+c_{sx}^2)\theta_x], \quad (17)$$

$$\delta_c' = -\left(\theta_c + \frac{h'}{2}\right) + 3\mathcal{H}\xi(1+w_x)\frac{\rho_x}{\rho_c+\rho_x} \times \left[-\delta_x + \frac{\rho_c\delta_c+\rho_x\delta_x}{\rho_c+\rho_x} - \frac{\theta+h'/2}{3\mathcal{H}}\right], \quad (18)$$

$$\theta_c' = -\mathcal{H}\theta_c. \quad (19)$$

Finally, we consider the third interaction model (IDE 3), with the choices $\alpha = -1$, $\beta = 0$, and this leads to the coupling

$$Q = 3H\xi(1+w_x)\frac{\rho_x^2}{\rho_c},$$

which gives rise to the variation $\delta Q = Q[(-\delta_c + 2\delta_x + (\theta + h'/2)/(3\mathcal{H})]$, and consequently, it is possible to find

[1]The conservation equations (1) and (2) can, respectively, be rewritten as $\rho_m' + 3\rho_m = -\bar{Q}$ and $\rho_x' + 3(1+w_x)\rho_x = \bar{Q}$, where $\bar{Q} = Q/H$ and the prime is taken with respect to the lapse function $N = \ln a$.

the perturbation equations of dark energy and dark matter, respectively, as

$$\delta_x' = -(1+w_x)\left(\theta_x + \frac{h'}{2}\right) - 3\mathcal{H}(c_{sx}^2 - w_x)\left[\delta_x + 3\mathcal{H}(1+w_x)\frac{\theta_x}{k^2}\right] + 3\mathcal{H}\xi(1+w_x)\frac{\rho_x}{\rho_c}\left[-\delta_c + 2\delta_x + \frac{\theta + h'/2}{3\mathcal{H}} + 3\mathcal{H}(c_{sx}^2 - w_x)\frac{\theta_x}{k^2}\right], \tag{20}$$

$$\theta_x' = -\mathcal{H}(1 - 3c_{sx}^2)\theta_x + \frac{c_{sx}^2}{(1+w_x)}k^2\delta_x + 3\mathcal{H}\xi\frac{\rho_x}{\rho_c}[\theta_c - (1+c_{sx}^2)\theta_x], \tag{21}$$

$$\delta_c' = -\left(\theta_c + \frac{h'}{2}\right) + 3\mathcal{H}\xi(1+w_x)\frac{\rho_x^2}{\rho_c^2}\left[2\delta_c - 2\delta_x - \frac{\theta + h'/2}{3\mathcal{H}}\right], \tag{22}$$

$$\theta_c' = -\mathcal{H}\theta_c. \tag{23}$$

We analyze these three interaction models using the latest observational data and discuss their large-scale stability.

III. OBSERVATIONAL DATA SETS

To constrain the three interacting models (IDE 1-3) we use observational data from different astronomical sources, as follows:

(1) *Cosmic microwave background observations (CMB):* We use CMB data from the Planck 2015 measurements [65,66], where we combine the full likelihoods C_l^{TT}, C_l^{EE}, C_l^{TE} with low-l polarization $C_l^{TE} + C_l^{EE} + C_l^{BB}$, which is notationally the same as the "PlanckTT, TE, EE + lowP" of Ref. [66].

(2) *Supernovae type Ia:* Supernovae type Ia are the first geometric sample to infer the accelerating phase of the universe and so far serve as one of the best samples to analyze any dark-energy model. In this work we use the latest SNIa sample, known as joint light curve analysis (JLA) samples [67] comprising 740 data points in the redshift range $0.01 \leq z \leq 1.30$.

(3) *Baryon acoustic oscillation (BAO) distance measurements:* For this data set, we use four BAO points—the 6dF Galaxy Survey (6dFGS) measurement at $z_{\rm eff} = 0.106$ [68], the Main Galaxy Sample of Data Release 7 of Sloan Digital Sky Survey (SDSS-MGS) at $z_{\rm eff} = 0.15$ [69], and the CMASS and LOWZ samples from the latest Data Release 12 (DR12) of the Baryon Oscillation Spectroscopic Survey (BOSS) at $z_{\rm eff} = 0.57$ [70] and $z_{\rm eff} = 0.32$ [70].

(4) *Redshift-space distortion:* We employ two RSD measurements, which include the CMASS sample with an effective redshift of $z_{\rm eff} = 0.57$ and the LOWZ sample with an effective redshift of $z_{\rm eff} = 0.32$ [71].

(5) *Weak lensing (WL):* We use the weak gravitational lensing data from Canada-France-Hawaii Telescope Lensing Survey (CFHTLenS) [72,73].

(6) *Cosmic chronometers (CC):* The Hubble parameter measurements from most old and passively evolving galaxies, known as cosmic chronometers have been considered as potential candidates to probe the nature of dark energy due to their model-independent measurements. For a detailed description on how one can measure the Hubble parameter values at different redshifts through this CC approach, and its usefulness, we refer to [74]. Here, we use 30 measurements of the Hubble parameter at different redshifts within the range $0 < z < 2$.

(7) *Local value of the Hubble constant (H_0):* We include the local value of the Hubble parameter which yields $H_0 = 73.24 \pm 1.74$ km/s/Mpc with 2.4% precision [75].

IV. RESULTS OF THE ANALYSIS

For the three interacting dark-energy models above, we consider the following eight-dimensional parameter space (see [76]):

$$P \equiv \{\Omega_b h^2, \Omega_c h^2, \Theta_S, \tau, w_x, \xi, n_s, \log[10^{10} A_S]\},$$

where $\Omega_b h^2$ and $\Omega_c h^2$ stand for the density of baryons and the dark matter, respectively; $\Theta_S = 100\theta_{MC}$ is the ratio of sound horizon to the angular diameter distance; τ is the optical depth; w_x is the equation-of-state parameter of dark energy; ξ is the coupling parameter; n_s is the scalar spectral index; and A_s represents the amplitude of the initial power spectrum. The priors of the basic model parameters are shown in the second column of Table I. The recent value of the Hubble constant $H_0 = 73.24 \pm 1.74$ km/s/Mpc [75] is used as a prior. Here, we note that the sound speed of dark-energy perturbations, c_{sx}, plays an important role in the large-scale dynamics. For stable perturbations of dark energy, one must have $c_{sx}^2 > 0$. Since we have assumed a constant equation-of-state parameter for the dark energy, if dark energy is an adiabatic fluid, then one can see that $c_{sx}^2 = c_{ax}^2 = w_x < 0$. This means that the sound speed of dark-energy perturbations becomes imaginary, and consequently, this leads to instabilities in the dark-energy evolution. Here, we assume $c_{sx}^2 = 1$, the sound speed for quintessence following the earlier studies in Refs. [27–29].

TABLE I. The table summarizes the mean values of the free and derived cosmological parameters with their errors at 68.3% and 95.4% confidence regions for IDE 1: $Q = 3H\xi(1+w_x)\rho_x$, IDE 2: $Q = 3H\xi(1+w_x)\rho_c\rho_x/(\rho_c+\rho_x)$, and IDE 3: $Q = 3H\xi(1+w_x)\rho_x^2/\rho_c$ using the combined analysis CMB + BAO + JLA + RSD + WL + CC + H_0. We note that $\Omega_{m0} = \Omega_{c0} + \Omega_{b0}$.

Parameters	Priors	IDE 1	Best fit	IDE 2	Best fit	IDE 3	Best fit
$\Omega_b h^2$	[0.005, 0.1]	$0.0223^{+0.0001+0.0003}_{-0.0001-0.0003}$	0.0222	$0.0223^{+0.0001+0.0003}_{-0.0002-0.0003}$	0.0222	$0.0223^{+0.0002+0.0003}_{-0.0001-0.0003}$	0.0222
$\Omega_c h^2$	[0.01, 0.99]	$0.1183^{+0.0014+0.0030}_{-0.0014-0.0029}$	0.1185	$0.1182^{+0.0013+0.0025}_{-0.0012-0.0027}$	0.1186	$0.1194^{+0.0022+0.0048}_{-0.0023-0.0047}$	0.1180
$100\theta_{MC}$	[0.5, 10]	$1.0406^{+0.0003+0.0006}_{-0.0003-0.0006}$	1.0403	$1.0406^{+0.0004+0.0006}_{-0.0003-0.0007}$	1.0408	$1.0406^{+0.0003+0.0006}_{-0.0003-0.0006}$	1.0406
τ	[0.01, 0.8]	$0.0663^{+0.0161+0.0315}_{-0.0162-0.0319}$	0.0762	$0.0662^{+0.0154+0.0318}_{-0.0178-0.0298}$	0.0514	$0.0682^{+0.0168+0.0317}_{-0.0170-0.0316}$	0.0699
n_s	[0.5, 1.5]	$0.9760^{+0.0036+0.0071}_{-0.0038-0.0070}$	0.9778	$0.9763^{+0.0044+0.0085}_{-0.0044-0.0087}$	0.9717	$0.9762^{+0.0038+0.0079}_{-0.0042-0.0074}$	0.9794
$\ln(10^{10}A_s)$	[2.4, 4]	$3.0722^{+0.0311+0.0605}_{-0.0288-0.0616}$	3.0945	$3.0714^{+0.0302+0.0622}_{-0.0341-0.0607}$	3.0414	$3.0747^{+0.0333+0.0624}_{-0.0332-0.0623}$	3.0747
w_x	$[-2, 0]$	$-1.0230^{+0.0329+0.0527}_{-0.0257-0.0603}$	−1.0210	$-1.0247^{+0.0289+0.0895}_{-0.0302-0.0841}$	−1.0374	$-1.0275^{+0.0228+0.0603}_{-0.0318-0.0509}$	−1.0134
ξ	[0, 1]	$0.0360^{+0.0091+0.0507}_{-0.0360-0.0360}$	0.0436	$0.0433^{+0.0062+0.0744}_{-0.0433-0.0433}$	0.0086	$0.1064^{+0.0437+0.1413}_{-0.1064-0.1064}$	0.1080
H_0	73.24 ± 1.74	$68.4646^{+0.8199+1.3348}_{-0.7380-1.3616}$	68.1714	$68.5099^{+0.8529+2.0520}_{-0.9264-1.7640}$	68.6939	$68.5420^{+0.7817+1.3760}_{-0.6763-1.4114}$	68.3716
Ω_{m0}	⋯	$0.3014^{+0.0070+0.0139}_{-0.0077-0.0141}$	0.3042	$0.3008^{+0.0082+0.0155}_{-0.0078-0.0163}$	0.2997	$0.3030^{+0.0063+0.0126}_{-0.0062-0.0124}$	0.3014
σ_8	⋯	$0.8156^{+0.0121+0.0246}_{-0.0137-0.0244}$	0.8249	$0.8166^{+0.0134+0.0300}_{-0.0166-0.0280}$	0.8096	$0.8051^{+0.0231+0.0336}_{-0.0185-0.0396}$	0.8068

In fact, with the assumption of $c_{sx}^2 = 1$, or close to 1, the dark energy does not cluster on the sub-Hubble scale. The dark-matter velocity perturbation equation is the same as in the uncoupled case, so we can consistently set $\theta_c = 0$ [27] since there is no momentum transfer in the rest frame of dark matter. Here, in order to study the effects of the interaction rate on the angular CMB power spectra, we modified the publicly available CAMB package [77], which is included in CosmoMC [78], to calculate the anisotropic power spectrum of the CMB.

This allows us to analyze the results of global fitting for the three different interaction models, namely, IDE 1: $Q = 3H\xi(1+w_x)\rho_x$, IDE 2: $Q = 3H\xi(1+w_x)\rho_c\rho_x/(\rho_c+\rho_x)$, and IDE 3: $Q = 3H\xi(1+w_x)\rho_x^2/\rho_c$.

Table I summarizes the main observational results extracted from all three interacting dark-energy models using the combined analysis CMB + BAO + JLA + RSD + WL + CC + H_0. In the following, we describe the behavior of each interacting fluid model in detail.

(i) IDE 1: In Fig. 1, we display the 68.3% and 95.4% confidence-level (C.L.) contour plots for different combinations of the free parameters of this model as well as the one-dimensional posterior distribution for each parameter. From the analysis, one finds that the model predicts a very small coupling in the dark sectors, with $\xi = 0.0360^{+0.0091}_{-0.0360}$ at 68.3% C.L. Also, as one can see, a zero value for ξ (i.e., no interaction) is allowed at 68.3% C.L. This implies that within 68.3% C.L., our interaction model can recover the noninteracting w_xCDM model. But, our analysis also shows that the equation of state of dark energy, w_x, can cross the phantom dividing line, with $w_x = -1.0230^{+0.0329}_{-0.0257}$ at 68.3% C.L. with the best fit value $w_x = -1.0210$. Although, at the 68.3% C.L., w_x could be greater than "−1," this means that its quintessential character cannot be excluded—at least according to the current observational data employed in this analysis. However, we note that numerical values of both mean and best fit values of w_x are close to the cosmological constant limit of $w_x = -1$. Thus, from the constraints on the coupling strength, as well as the equation of state for dark energy, one finds that the observational data favor a very small interaction in the dark sector, and the model for the background evolution displays a close match to the ΛCDM cosmology. We also find that, at the perturbative level, IDE 1 cannot be distinguished from the ΛCDM cosmology. In Figs. 2 and 3, we have described the angular power spectra of the CMB temperature anisotropy and the matter power spectra for different values of w_x and ξ. We see that a very slight deviation is observed at the highest peak of the plot (right-hand panel of Fig. 2) for a higher coupling strength of $\xi = 0.8$. A very similar observation can be made about the matter power spectra (right-hand panel of 3) for $\xi = 0.8$. However, overall, the model does not show any significant deviation from ΛCDM even for such a high coupling strength. Similarly, as w_x deviates from −1 towards the quintessence regime, a very slight deviation from the ΛCDM cosmology is observed, although it is not significant either. Further, in Fig. 4, we have displayed the two-dimensional marginalized posterior distribution for the parameters (w_x, ξ) using the combined analysis mentioned above. The points in Fig. 4 are the samples from the chains of the combined analysis that have been colored by the values of H_0. From this figure, it is seen that the higher values of H_0 favor the phantom

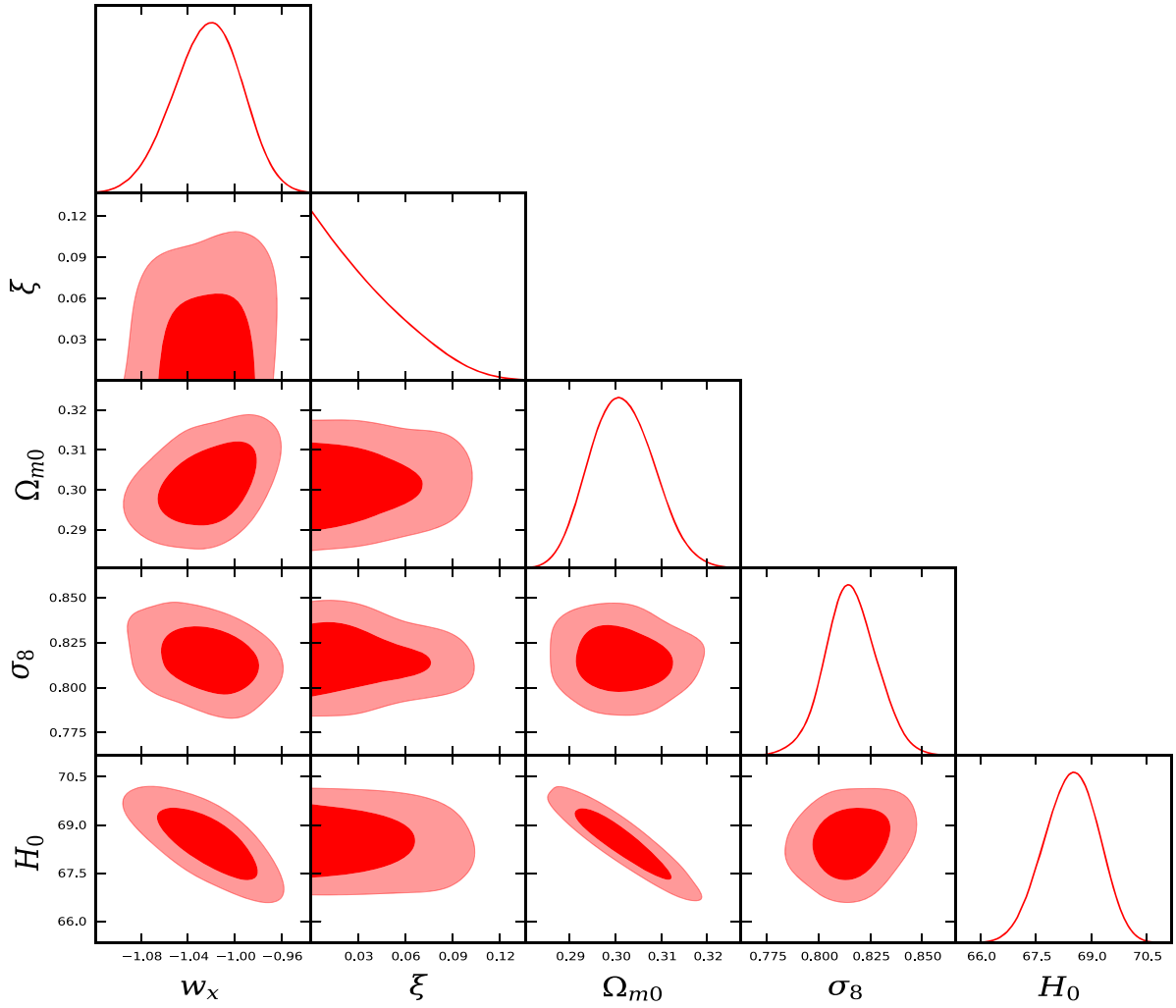

FIG. 1. The figure displays the 68.3% and 95.4% confidence-region contour plots for IDE 1 using the combined analysis CMB + BAO + JLA + RSD + WL + CC + H_0. Here, $\Omega_{m0} = \Omega_{c0} + \Omega_{b0}$.

regime, $w_x < -1$, while the lower values of H_0 favor the quintessence dark energy, i.e., $w_x > -1$. In fact, a shifting from phantom to quintessence dark energy is displayed as the Hubble parameter values decrease from higher values. Furthermore, we can also see that a nonzero interaction might be useful to ease the tension on H_0 created by the ΛCDM-based Planck estimation ($H_0 = 67.27 \pm 0.66$ km s^{-1} Mpc^{-1}) [1] and the local measurements by Riess *et al.* ($H_0 = 73.24 \pm 1.74$ km s^{-1} Mpc^{-1}) [75]. From our analysis, we find that the introduction of a coupling into the dark sector gives $H_0 = 68.4646^{+0.8199+1.3348+1.6568}_{-0.7380-1.3616-1.8747}$, which shows that the coupling does produce a shift of the Hubble parameter towards higher values, and consequently, the tension on H_0 might be eased in the presence of the interaction. The easing of the H_0 tension in the presence of an interaction in the dark sector has also been noticed in some earlier works [21,79,80] with some different interactions, and thus it might be considered an interesting outcome of such a w_xCDM + ξ scenario. One can also see that the σ_8 value extracted from this model matches with the Planck estimation [1] when lensing is added to either Planck TT + lowP or Planck TT, TE, EE + lowP. This means that the estimated values of σ_8 are $\sigma_8 = 0.8149 \pm 0.0093$ (Planck TT+lowP +lensing) [1] and $\sigma_8 = 0.8150 \pm 0.0087$ (Planck TT, TE, EE + lowP + lensing) [1]. The external data BAO+JLA+H_0 added to both of these data (Planck TT + lowP and Planck TT, TE, EE + lowP) agree with the same estimation.

(ii) IDE 2: In Fig. 5, we display the 68.3% and 95.4% confidence-level (C.L.) contour plots for different combinations of the free parameters of this model as well as the one-dimensional posterior distribution for each parameter. The results for IDE 2 are quite similar to IDE 1. The coupling parameter for this model is constrained to be ($\xi = 0.0433^{+0.0062}_{-0.0433}$ at 68.3% C.L.) from the combined analysis, and we also notice that a zero value of ξ is allowed at the

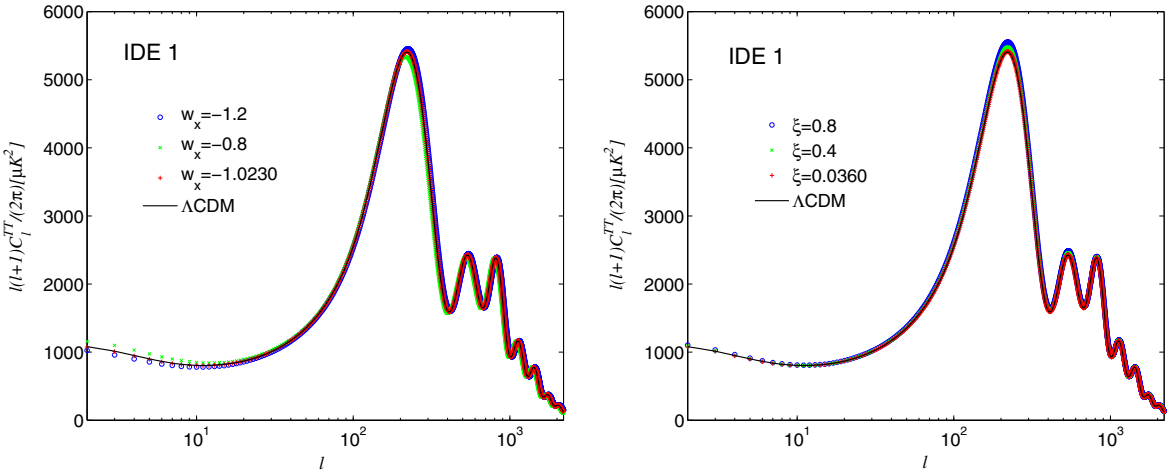

FIG. 2. The plots show the angular CMB temperature power spectra of IDE 1 compared to the standard ΛCDM cosmology using the combined analysis CMB + BAO + JLA + RSD + WL + CC + H_0. In the left panel we show different angular CMB spectra for different values of w_x including its mean value obtained from the above combined analysis, while the right panel shows a replica of the left panel but for different values of the coupling parameter ξ, including its mean value from the same combined analysis.

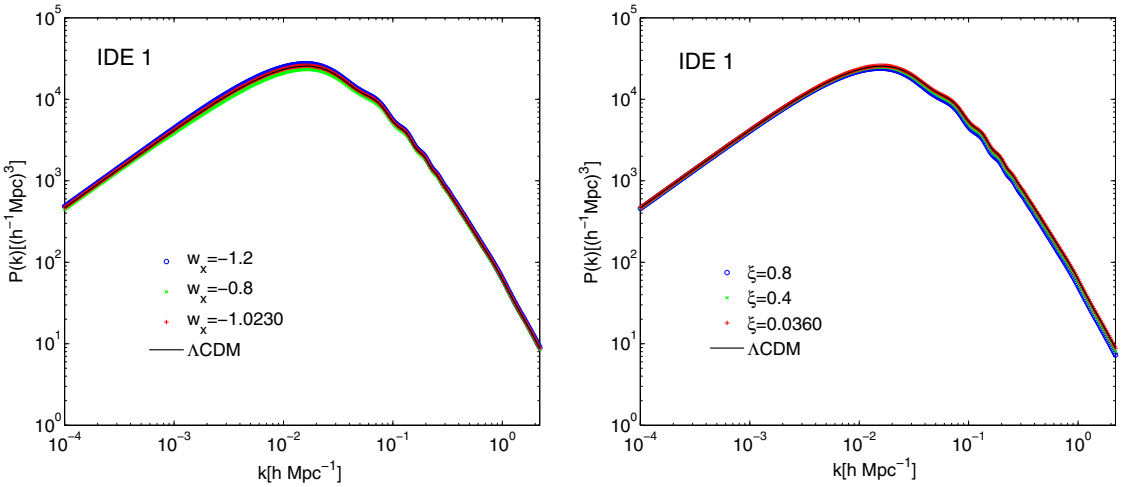

FIG. 3. The figure shows the behavior of the matter power spectra of IDE 1 compared to the ΛCDM cosmology for the combined observational analysis CMB + BAO + JLA + RSD + WL + CC + H_0. In the left panel we use different values of the dark-energy equation of state w_x, while in the right panel we vary the coupling parameter ξ.

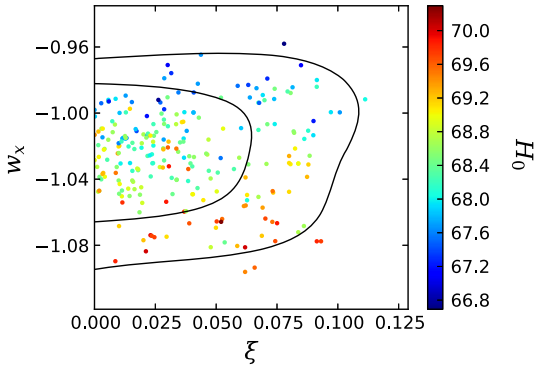

FIG. 4. MCMC samples in the (w_x, ξ) plane colored by the Hubble constant value H_0 for IDE 1 analyzed with the combined analysis CMB + BAO + JLA + RSD + WL + CC + H_0.

68.3% C.L. This means the noninteracting w_xCDM cosmology is still permitted, while the observational data always favor $\xi \neq 0$. In addition, we find that this interacting scenario allows the equation of state for dark energy to go over the phantom divide boundary of -1. The best fit ($w_x = -1.0374$) and the mean value of w_x ($= -1.0247^{+0.0289}_{-0.0302}$ at 68.3% C.L.) are the characteristics of a phantom dark energy. However, at the 68.3% C.L., the possibility of $w_x > -1$ is permitted, at least from the present observational data. Furthermore, in Figs. 6 and 7 we have plotted the CMB temperature anisotropy spectra and the matter power spectra for a wide range of w_x and ξ, and both these plots indicate that IDE 2 does not deviate much from the standard Λ-cosmology. In fact,

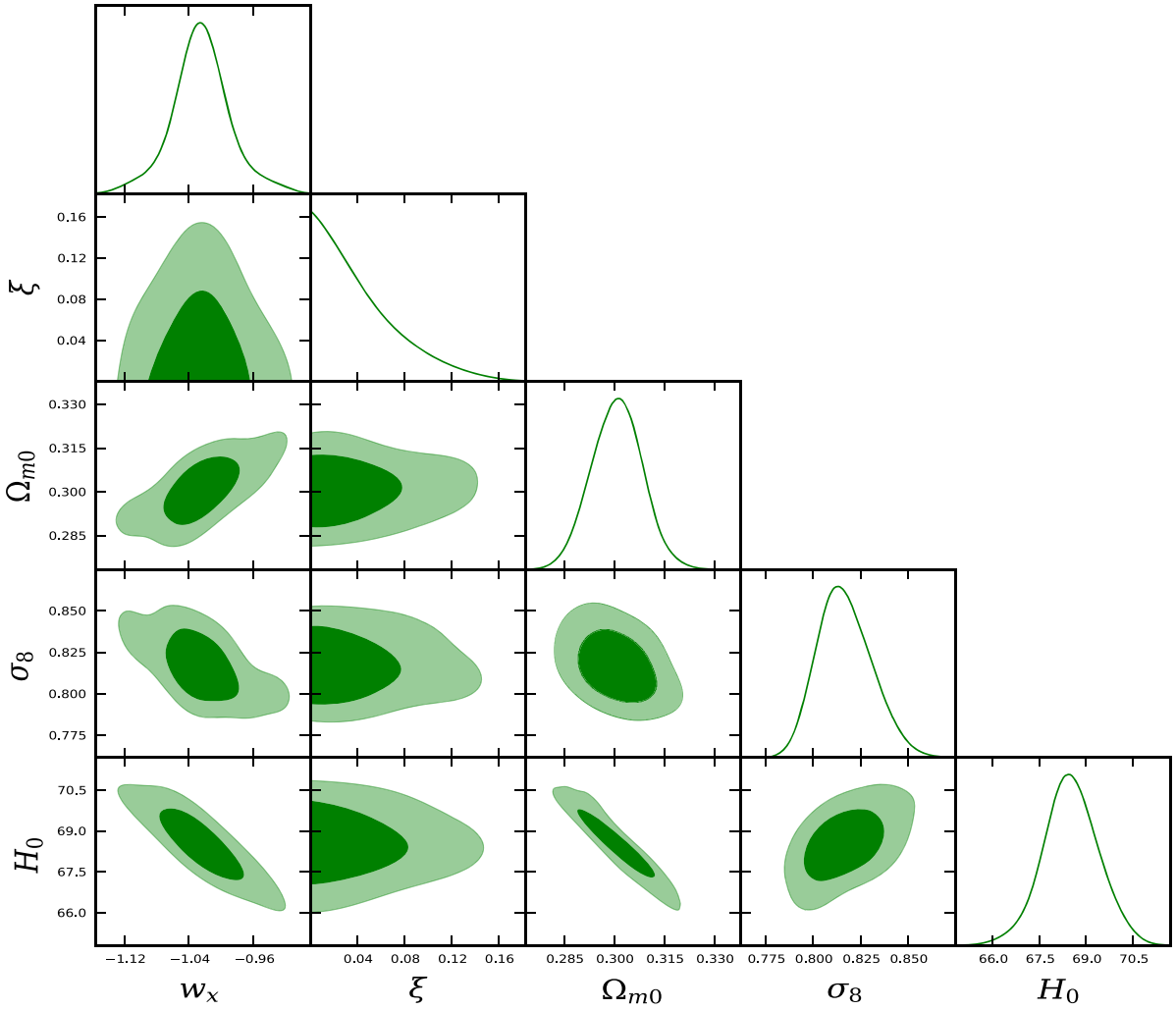

FIG. 5. The figure displays the 68.3% and 95.4% confidence-region contour plots for different combinations of the free parameters of IDE 2 using the combined analysis CMB + BAO + JLA + RSD + WL + CC + H_0. Here, $\Omega_{m0} = \Omega_{c0} + \Omega_{b0}$.

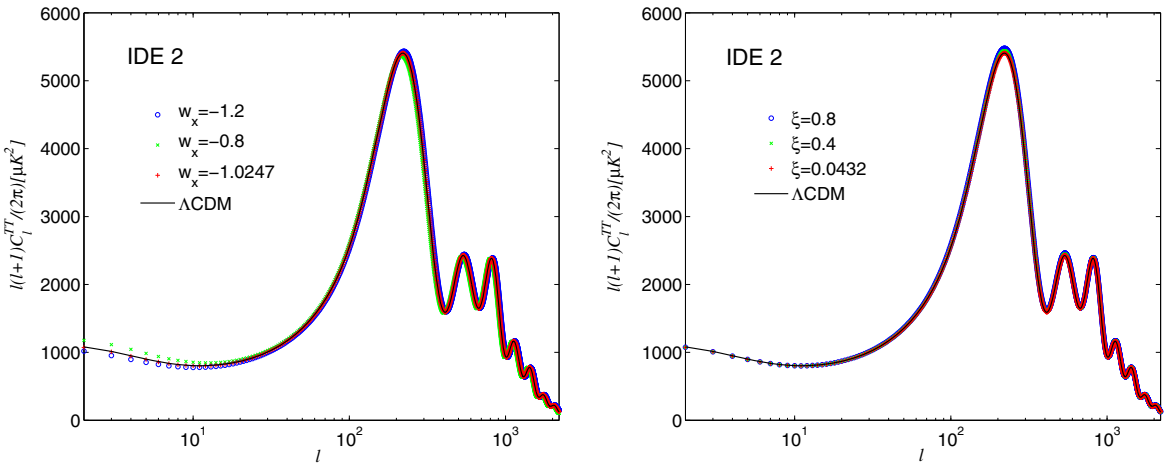

FIG. 6. The plots show the angular CMB temperature power spectra of IDE 2 compared to the standard ΛCDM cosmology using the combined analysis CMB + BAO + JLA + RSD + WL + CC + H_0. In the left panel we show different angular CMB spectra for different values of w_x including its mean value obtained from the combined analysis, while the right panel shows a replica of the left panel but for different values of the coupling parameter ξ including its mean value from the same combined analysis.

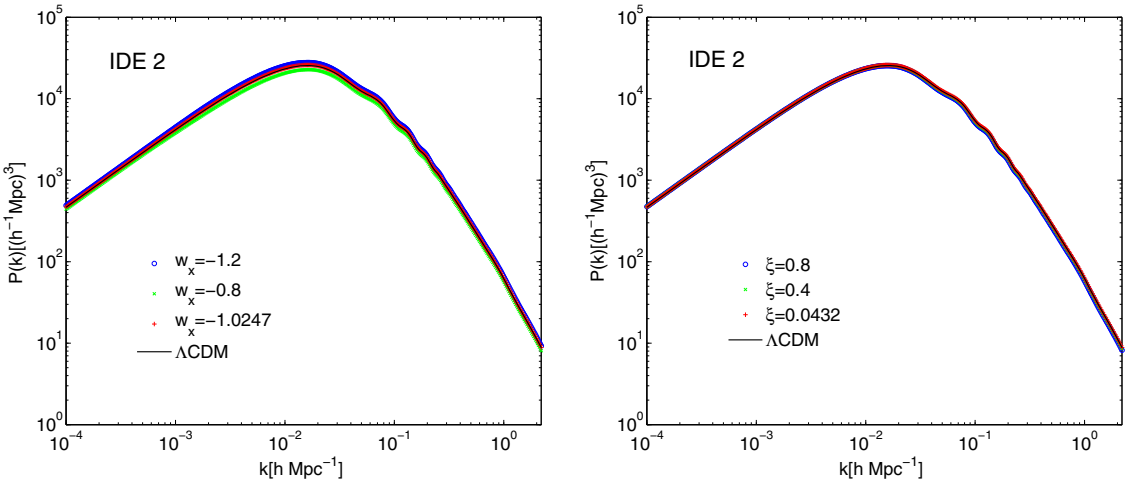

FIG. 7. The figure shows the behavior of the matter power spectra of IDE 2 compared to the ΛCDM cosmology for CMB + BAO + JLA + RSD + WL + CC + H_0. In the left panel we use different values of the dark-energy equation of state w_x, while in the right panel we vary the coupling parameter ξ.

we observe that the deviation from the Λ-cosmology for the strong coupling, $\xi = 0.8$, is weaker in respect to the deviation for the same coupling strength observed in IDE 1. A similar argument for w_x holds true as for IDE 1. In Fig. 8 we also show the two-dimensional marginalized posterior distribution for the parameters (w_x, ξ) using the combined analysis mentioned above. The points in Fig. 8 are the samples from the chains of the combined analysis that have been colored by the values of H_0. We find similar behavior as in IDE 1. This means that higher values of H_0 favor the phantom regime $w_x < -1$, while lower values of H_0 favor the quintessence dark energy, i.e., $w_x > -1$. The shift from phantom to quintessence dark energy is displayed as the Hubble parameter values decrease from higher values. We now return to the estimation of the Hubble parameter in order to see whether this model could also ease the tension on H_0 in a similar fashion to that observed in IDE 1. The estimated value from our analysis is $H_0 = 68.5099^{+0.8529+2.0520+2.1279}_{-0.9264-1.7640-2.4521}$. One can clearly see that the inclusion of the coupling shifts the Hubble parameter towards higher values; however, in comparison to IDE 1, the shifting is now slightly higher. Certainly, the tension on H_0 might be released in a similar fashion. Thus, at the statistical level, this model resembles IDE 1. Moreover, the estimated value of σ_8 for this model also matches the ΛCDM-based Planck estimate [1], in the presence of lensing where $\sigma_8 = 0.8149 \pm 0.0093$ (Planck TT + lowP + lensing) [1] and $\sigma_8 = 0.8150 \pm 0.0087$ (Planck TT, TE, EE + lowP + lensing) [1]. The observational constraints in the presence of the other data, for instance BAO + JLA + H_0, return similar fits to σ_8 [1]. Thus, we see that this interaction model is close to the ΛCDM cosmology.

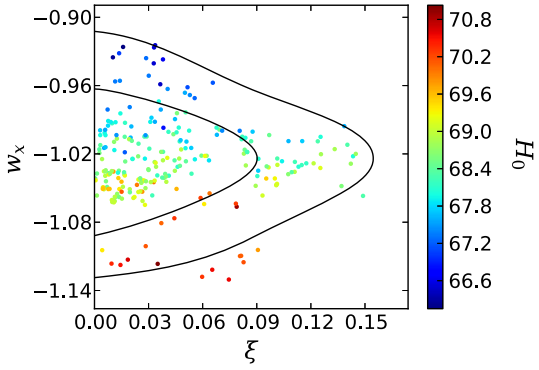

FIG. 8. MCMC samples in the (w_x, ξ) plane colored by the Hubble constant value H_0 for IDE 2 analyzed with the combined analysis CMB + BAO + JLA + RSD + WL + CC + H_0.

(iii) IDE 3: In Fig. 9, we display the 68.3% and 95.4% confidence-level (C.L.) contour plots for different combinations of the free parameters of this model as well as the one-dimensional posterior distribution for each parameter. The observational constraints on IDE 3 display some different properties from those of IDE 1 and IDE 2. We find that the coupling parameter ξ is comparatively high ($\xi = 0.1064^{+0.0437}_{-0.1064}$ at 68.3% C.L.), unlike in the two other interaction models (68.3% C.L. constraints on the coupling strength are $\xi = 0.0360^{+0.0091}_{-0.0360}$ for IDE 1 while $\xi = 0.0433^{+0.0062}_{-0.0433}$ for IDE 2), although its zero value is still marginally allowed at the 68.3% C.L. The best fit and the mean values of w_x describe a phantom dark energy. The numerical values of the best fit, as well as the mean values of the dark-energy equation of state, are, respectively, $w_x = -1.0134$ and $w_x = -1.0275^{+0.0228}_{-0.0318}$ (at 68.3% C.L.). It is interesting to

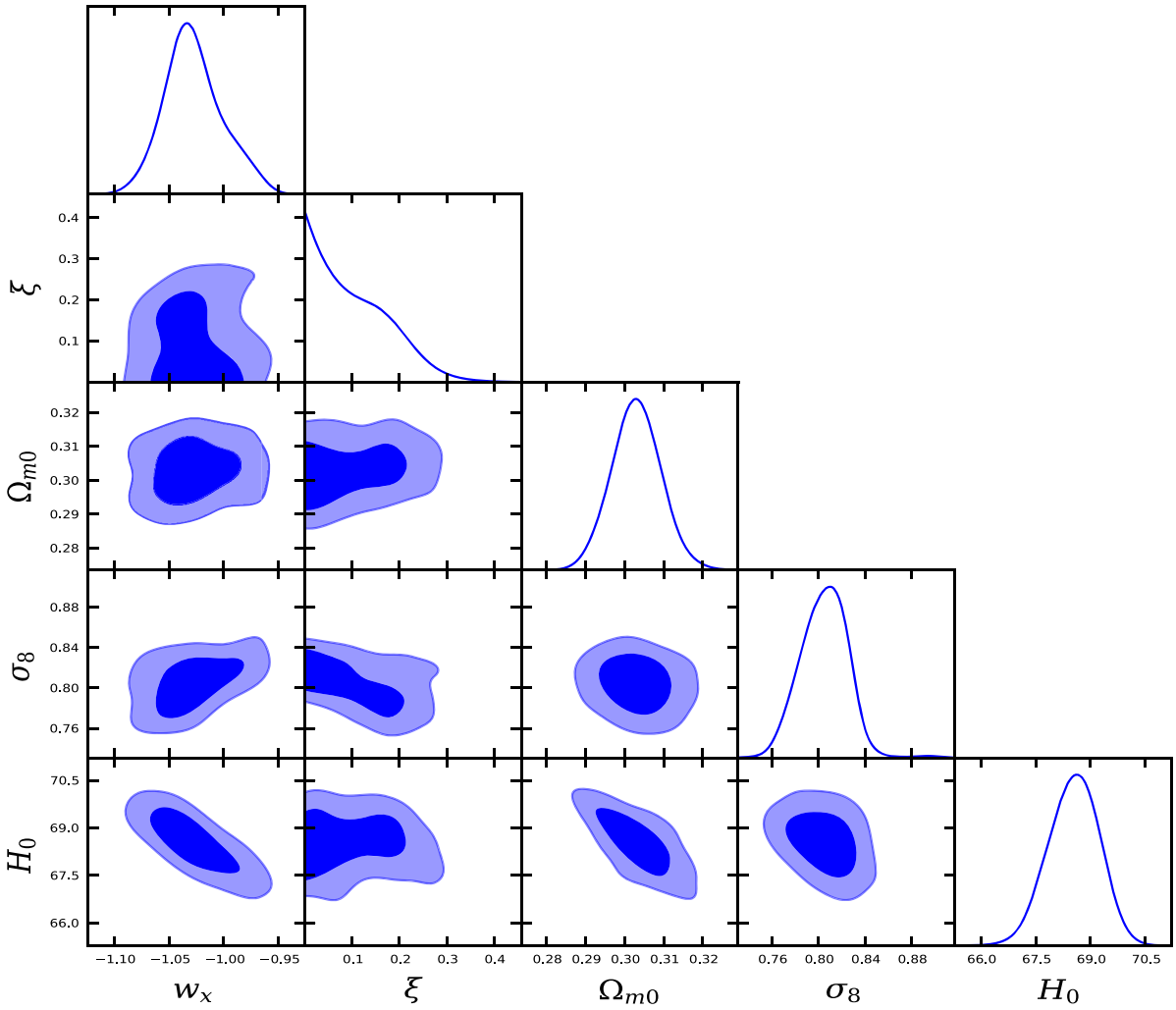

FIG. 9. The figure displays the 68.3% and 95.4% confidence-region contour plots for IDE 3 using the combined analysis CMB + BAO + JLA + RSD + WL + CC + H_0. Here, $\Omega_{m0} = \Omega_{c0} + \Omega_{b0}$.

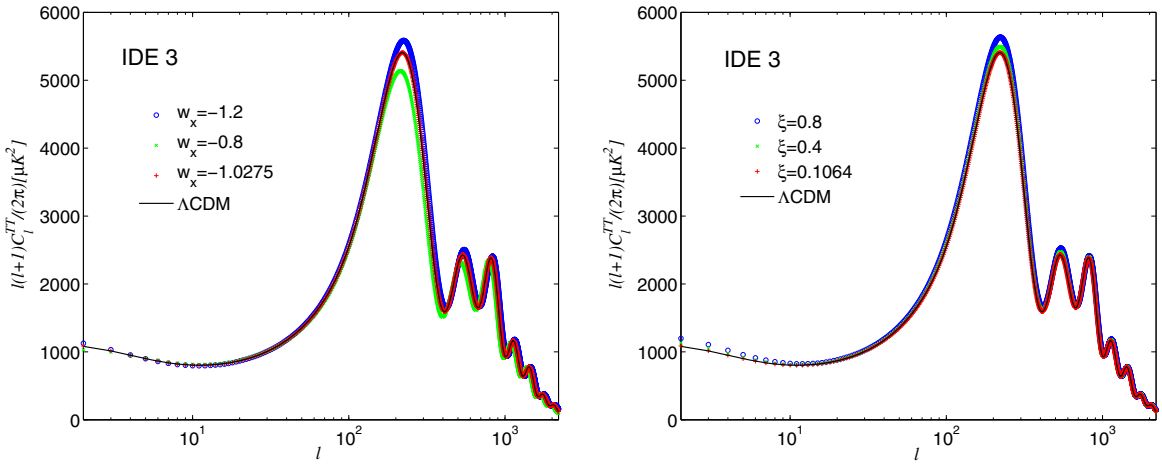

FIG. 10. The plots show the angular CMB temperature power spectra of IDE 3 compared to the standard ΛCDM cosmology for the analysis CMB + BAO + JLA + RSD + WL + CC + H_0. In the left panel we show different angular CMB spectra for different values of w_x including its mean value obtained from the combined analysis, while the right panel shows a replica of the left panel but for different values of the coupling parameter ξ including its mean value from the same combined analysis.

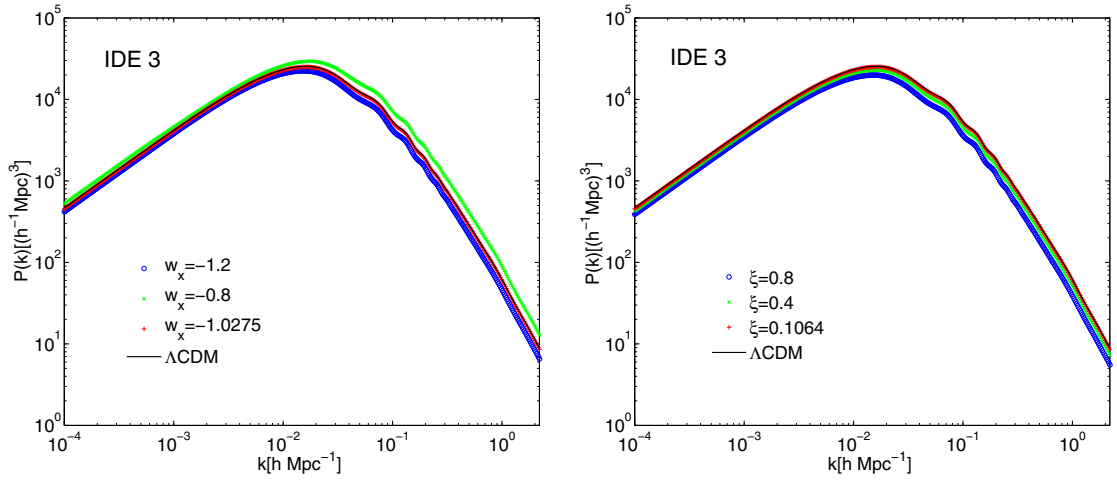

FIG. 11. The figure shows the behavior of the matter power spectra of IDE 3 compared to the ΛCDM cosmology for CMB + BAO + JLA + RSD + WL + CC + H_0. In the left panel we use different values of the dark-energy equation of state w_x, while in the right panel we vary the coupling parameter ξ.

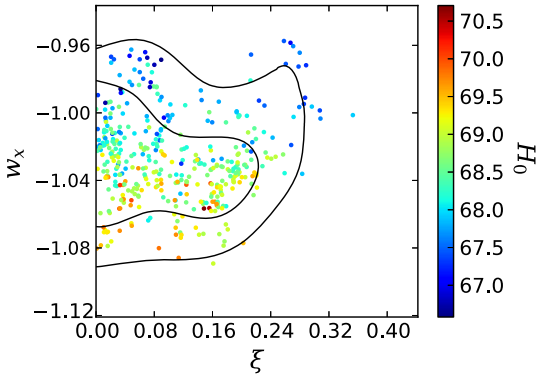

FIG. 12. MCMC samples in the (w_x, ξ) plane colored by the Hubble constant value H_0 for IDE 3 analyzed with the combined analysis CMB + BAO + JLA + RSD + WL + CC + H_0.

mention that, at 68.3% C.L., the dark-energy equation of state w_x strictly shows phantom behavior. However, at the 95.4% confidence level, w_x could still be greater than -1 ($w_x = -1.0275^{+0.0603}_{-0.0509}$ at 95.4% C.L.), which means the quintessential regime is not excluded at all, at least with the present data. Now, following the same trend as in IDE 1 and IDE 2, in Figs. 10 and 11, respectively, we show the CMB temperature anisotropy spectra and the matter power spectra for a wide range of w_x and the coupling strength ξ. From both the figures, we see that the model shows a clear difference from the Λ-cosmology and hence from the other two interaction models. However, it is also true that such differences observed in Figs. 10 and 11 are not significant enough, although a nonzero deviation from Λ-cosmology is clearly presented. The deviations in other cosmological parameters for this model can also be compared to IDE 1 and IDE 2. As one can see, a lower value of σ_8 ($= 0.8051^{+0.0231+0.0336}_{-0.0185-0.0396}$) is favored for this model unlike for the other two IDE models where the estimations are $\sigma_8 = 0.8156^{+0.0121+0.0246}_{-0.0137-0.0244}$ (IDE 1) and $\sigma_8 = 0.8166^{+0.0134+0.0300}_{-0.0166-0.0280}$ (IDE 2). This value also reflects a slight difference from the Planck estimate [1]. Thus, one can see that, according to the observations, this model shows a nonzero deviation from the Λ-cosmology with a phantom character within up to the 68.3% C.L. Now, concerning the tension on H_0 determinations, we find that IDE 3 may also ease such tension. This might be clear from the estimation of the Hubble parameter, $H_0 = 68.5420^{+0.7817+1.3760+1.6177}_{-0.6763-1.4114-1.9236}$, and by following similar arguments to those provided for IDE 1 and IDE 2. Finally, in Fig. 12, we plot the two-dimensional marginalized posterior distribution for the parameters (w_x, ξ) as we did for the models IDE 1 and IDE 2. The observational data are as described above. Overall, we find that IDE 3 follows a similar trend to IDE 1 and IDE 2. Indeed, this interaction model shows differences with respect to the other two interaction models, but such differences are small.

A. Comparisons of the IDE models

Let us provide a statistical comparison of the three IDE models. In order to visualize all three models in a single frame, in Fig. 13 we have provided the contour plots for different combinations of the model parameters. It is clearly seen that IDE 1 and IDE 2 have considerable overlap with each other, showing that these two models resemble each other, while IDE 3 is slightly different, which can be seen from the estimation of the coupling parameter, and also from the behavior of the dark-energy equation of state which retains its phantom character within 68.3% C.L. unlike the other two interaction models, namely, IDE 1 and

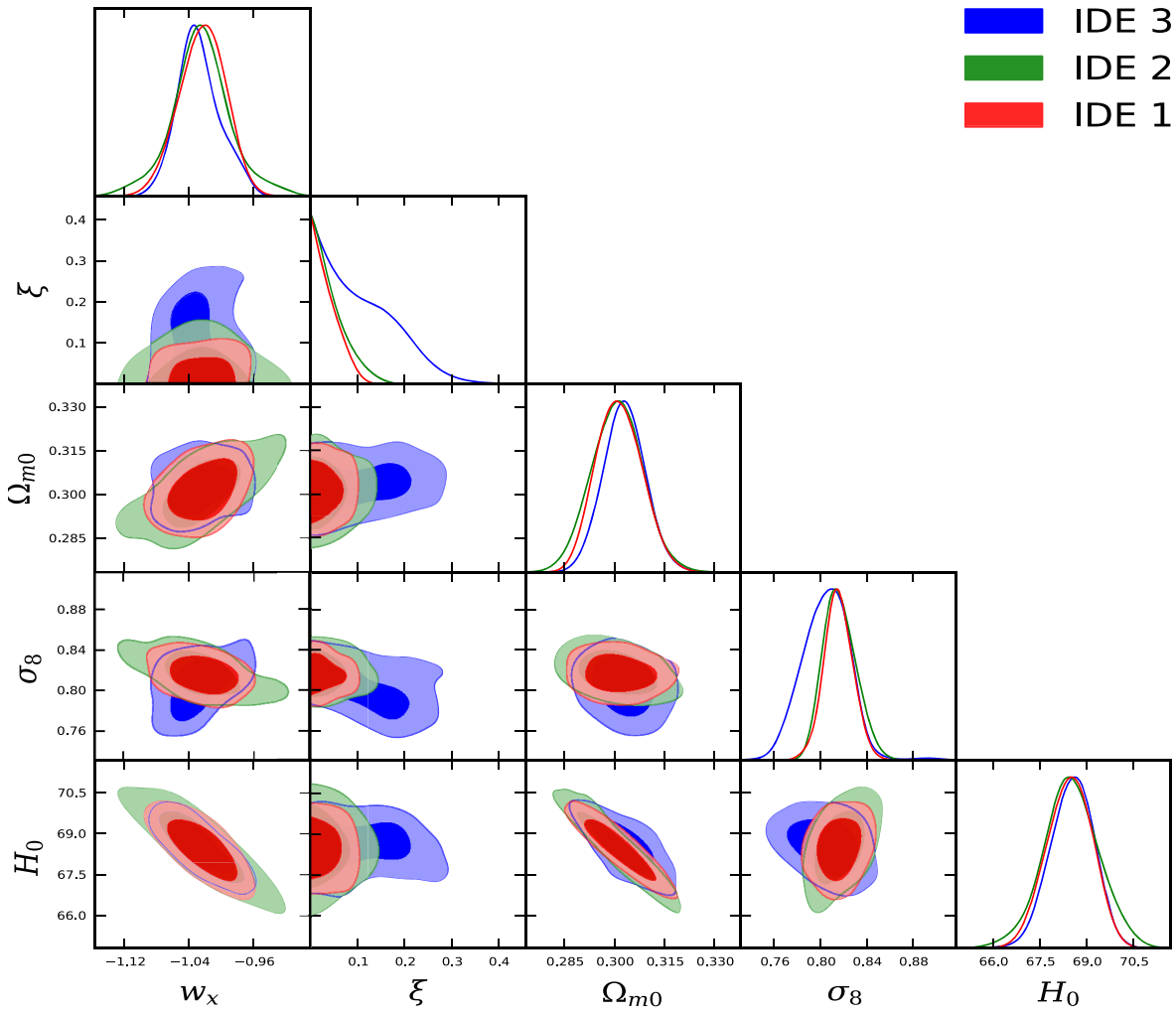

FIG. 13. The figure displays the 68.3% and 95.4% confidence-region contour plots for three interacting dark-energy models, namely, IDE 1, IDE 2, and IDE 3 using the combined analysis CMB + BAO + JLA + RSD + WL + CC + H_0. Here $\Omega_{m0} = \Omega_{c0} + \Omega_{b0}$.

IDE 2. Nevertheless, they share some common properties. The IDE models all favor a crossing of the phantom divide line. The mean values and the best fit values of the dark-energy equation of state all cross the -1 boundary. A striking feature of all of these interaction models is the alleviation of the tension between the different values of H_0 deduced from the local [75] and global measurements [1]. We find that the allowance of coupling in the dark sector is the main factor that shifts the Hubble parameter values toward its local measurement [75]. We note also that the alleviation of the tension on H_0 has been found earlier in the context of interacting dark energy [21,79,80] with some specific models. This might be considered one of the most interesting features of interacting dark-energy models.

From the analysis of large-scale structure it is seen from the evolution of the matter power spectra (see the right panel of Fig. 14) or the CMB temperature anisotropy (see the left panel of Fig. 14) that the models do not show any remarkable deviation from each other. Within 68.3% C.L., the current interacting models are very close to ΛCDM cosmology. Moreover, in Fig. 15 we have shown the qualitative evolution of the ratio Ω_m/Ω_r for all interacting models, and we have also compared the same evolution with the Λ-cosmology. We find that for very small coupling parameter values, the evolution of the quantity Ω_m/Ω_r is very close to that of ΛCDM cosmology. However, for larger values of $\xi(< 1)$, the deviation of course increases. This is prominent for IDE 3, and then for IDE 1, and after that for IDE 2 (see the subfigures in Fig. 15). But, the deviations for all three models are not significant enough to draw a decisive conclusion against the Λ-cosmology. We note that the evolution of Ω_m/Ω_r also tells us that IDE 3 is slightly different from the other two IDE models. We recall from the temperature and matter power spectra displayed in Figs. 10 and 11 that we noticed similar findings about IDE 3.

From the temperature anisotropy in the CMB TT spectra and also from the matter power spectra displayed for all models, the differences between the different models, as well as from the pure Λ-cosmology, are not strong. But, one can clearly show the differences between the models using

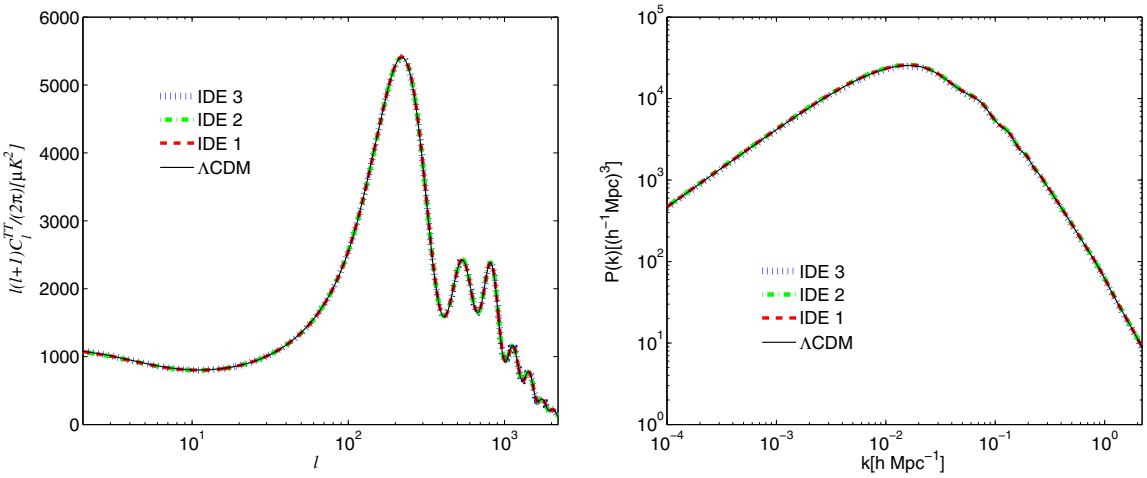

FIG. 14. CMB temperature anisotropy (left panel) and the matter power spectra (right panel) have been shown for three IDE models compared to the ΛCDM model, using the mean values of the free parameters obtained from the combined analysis CMB + BAO + JLA + RSD + WL + CC + H_0.

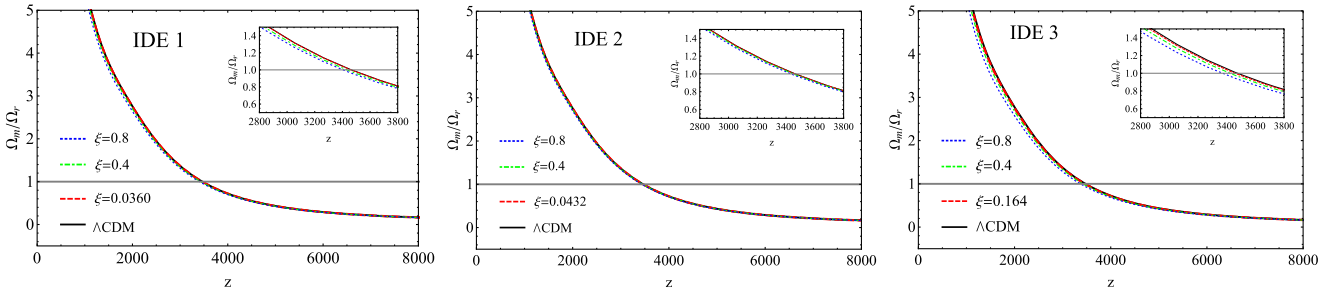

FIG. 15. The qualitative evolution of the ratio Ω_m/Ω_r (here $\Omega_m = \Omega_c + \Omega_b$) for the three IDE models has been shown for different values of the coupling parameter ξ and compared with the ΛCDM evolution. We note that the values $\xi = 0.0360$, $\xi = 0.0432$, and $\xi = 0.164$ are, respectively, the mean values of the coupling parameters obtained from the models IDE 1, IDE 2, and IDE 3 using the combined observational analysis CMB + BAO + JLA + RSD + WL + CC + H_0.

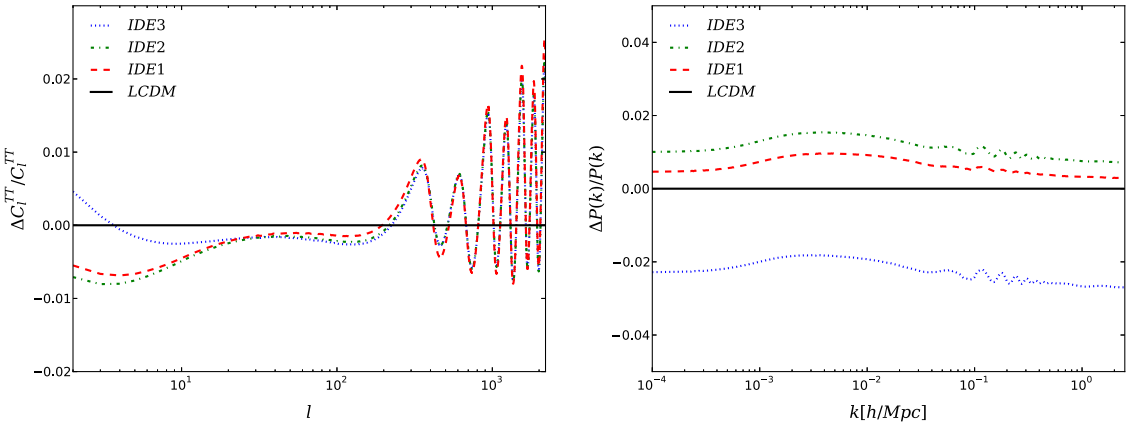

FIG. 16. The relative deviations of the IDE models from the Λ-cosmology through the CMB TT and matter power spectra have been shown using the mean values of the model parameters from the combined analysis CMB + BAO + JLA + RSD + WL + CC + H_0. One may notice that the models are also distinguished from one another.

the relative deviations of the models with respect to the base Λ-cosmological model. In order to depict the differences between the models, in Fig. 16 we have shown the relative deviations of the models from the pure Λ-cosmology in terms of the CMB TT spectra (left-hand panel of Fig. 16) and the matter power spectra (right-hand panel of Fig. 16) as well. One can clearly see that the deviations between the models exist, but such deviations are small.

Finally, we complete our comparisons with a brief remark. In Figs. 4, 8, and 12, we display the two-dimensional marginalized posterior distribution for the parameters (w_x, ξ) using the combined analysis of CMB + BAO + JLA + RSD + WL + CC + H_0. The points in Figs. 4, 8, and 12 are the samples from the chains of the combined analysis that have been colored by the values of H_0. We find that for all models, the higher values of H_0 favor the phantom regime $w_x < -1$, while the lower values of H_0 favor a quintessence dark energy, i.e., $w_x > -1$. A striking feature allowed by all the interacting fluid models is that, as the values of H_0 decrease, a clear shift in the dark-energy behavior, from phantom to quintessence, is observed, although the dark-energy equation of state still remains very close to the cosmological constant boundary.

V. SUMMARY AND CONCLUSIONS

Phenomenological interaction models for the transfer of energies in cosmological models have been widely investigated in recent years. They include a wide range of assumed interaction dependences, such as $Q \propto \rho_c$, $Q \propto \rho_x$, $Q \propto (\rho_c + \rho_x)$, and others. In order to impose observational constraints on these scenarios and evaluate the stability of the expanding universe models they require, some specific parametric space needs to be considered. For instance, if the dark-energy equation of state is described by w_x and the coupling parameter of the interaction is ξ, then the model is generally tested within two separate intervals, namely, $w_x \geq -1$ and $\xi \geq 0$ or $w_x \leq -1$ and $\xi \leq 0$. So, there exists a discontinuity in the testable range of the dark-energy equation of state.

In this paper we have provided a new technique to test some interacting models without restriction to any specific subintervals of the parameter space defining them. We carried out a general analysis of the inhomogeneous perturbations of a general interaction model linking dark energy and dark matter. We found that with the introduction of a new factor $(1 + w_x)$ in the background energy transfer, it is possible to test the whole space of the equation of state for dark energy with the observational data. We tested the scenarios using three different interaction models: $Q = 3H\xi(1 + w_x)\rho_x$, $Q = 3H\xi(1 + w_x)\rho_c\rho_x/(\rho_c + \rho_x)$, and $Q = 3H\xi(1 + w_x)\rho_x^2/\rho_c$. One can say that the inclusion of $(1 + w_x)$ into the energy transfer rate Q can be viewed as a transformation of the coupling parameter as $\xi \to \bar{\xi} = \xi(1 + w_x)$. Following this, the models can be viewed in terms of the transformed coupling parameter $\bar{\xi}$ as $Q = 3H\bar{\xi}\rho_x$, $Q = 3H\bar{\xi}\rho_c\rho_x/(\rho_c + \rho_x)$, and $Q = 3H\bar{\xi}\rho_x^2/\rho_c$. We employed the latest astronomical data from several independent sources, namely, the Planck 2015 cosmic microwave background anisotropy, baryon acoustic oscillation, joint light curves from type Ia supernovae, redshift-space distortions, weak gravitational lensing, and cosmic chronometers, together with the best local value of the Hubble constant. Using the Markov chain Monte Carlo algorithm we have constrained all three interaction scenarios. We find that in all three scenarios, the observational data favor a nonzero interaction between the dark sectors. In particular, for the first two IDE models, the observational data favor an almost zero interaction (the 68.3% C.L. constraints are $\xi = 0.0360^{+0.0091}_{-0.0360}$ for IDE 1 and $\xi = 0.0433^{+0.0062}_{-0.0433}$ for IDE 2), while the third one suggests a slightly higher interaction coupling strength ($\xi = 0.1064^{+0.0437}_{-0.1064}$ at 68.3% C.L.) in comparison to the IDE 1 and IDE 2 models. However, it is clear that within 68.3% C.L., all interaction models recover the no-interaction scenario (i.e., $\xi = 0$). This means that the observational data allow all IDE models to converge to the noninteracting w_xCDM model. Furthermore, the observational data also predict that the mean value, as well as the best fit value, of the dark-energy equation of state, w_x, both cross the phantom divide line. More precisely, the 68.3% C.L. constraints on the dark-energy equation of state for the IDE models are $w_x = -1.0230^{+0.0329}_{-0.0257}$ (for IDE 1), $w_x = -1.0247^{+0.0289}_{-0.0302}$ (for IDE 2), and $w_x = -1.0275^{+0.0228}_{-0.0318}$ (for IDE 3). As one can see, within 68.3% C.L., w_x is not so far from the cosmological constant boundary -1. We also observe that not all models exclude the possibility of $w_x > -1$. For IDE 1 and IDE 2, $w_x > -1$ is allowed in the 68.3% C.L., while for IDE 3, 95.4% C.L. shows this possibility. Overall, a significant feature of all these interaction models we find is that, from the analysis at the background level, none of our three interaction models can be distinguished from the Λ-cosmology. In fact, from the perturbative analysis, it is also quite difficult to distinguish between the models as well as distinguish them from the Λ-cosmology; of course, small deviations between any two models do exist, and all the models also differ from Λ-cosmology. Moreover, in all such models, we observe that the current tension on H_0 from different data sets can be relieved. This property of the interacting models could be a general one since some other recent articles make the same suggestion [79,80]. Finally, we found that a characteristic feature of all IDE models is that as the value of the Hubble constant decreases, the behavior of the dark-energy equation of state is shifted from phantom to quintessence type, with its equation of state very close to that of a simple cosmological constant at the present time.

We conclude our analysis with a comparison of the observational constraints with some of the proposed models, specifically with $Q \propto \rho_x$ and $Q \propto \rho_c\rho_x/(\rho_c + \rho_x)$.

We note that the analysis including the cosmological perturbations for the model $Q \propto \rho_x^2/\rho_c$ has not been performed in the past. The difference between the past and current analyses is that here we vary the dark-energy equation of state w_x within the interval $[-2, 0]$, and hence, it is expected to have slightly different results compared to the past analyses. In [30–33], the authors performed analyses for $w_x > -1$, which estimated the coupling parameter for the interaction model $Q = 3H\xi\rho_x$. In [30], the authors reported the coupling parameter ξ for two different sets of the combined analyses, which measured $\xi = 0.209^{+0.0711}_{-0.0403}$ at 1σ confidence level (for Planck + WMAP9 + SNIa + BAO) and $\xi = 0.00372^{+0.00768}_{-0.00372}$ at 1σ confidence level (for Planck + WMAP9 + SNIa + BAO + RSD) where the observational data are described in [30]. Thus, one can see that the inclusion of RSD into the other data significantly decreases the coupling strength. Similar analyses can be found in [31–33]. On the other hand, a recent analysis with $Q \propto \rho_x$, where the dark-energy equation-of-state parameter is constant and allowed to cross the phantom divide line (i.e., $w_x < -1$) [80], shows that within 2σ confidence level, the coupling parameter is nonzero ($\xi = -0.26^{+0.16}_{-0.12}$). Additionally, the interaction model $Q \propto \rho_x$ is tested when the dark energy represents the cosmological constant, i.e., for $w_x = -1$ (see the details in [81]). The analysis in [81] returned different fits from different observational data; in particular, within 1σ confidence level, $\xi = 0.036^{+0.114}_{-0.039}$ (Planck), $\xi = 0.020^{+0.048}_{-0.053}$ (Planck + BAO + SNIa), $\xi = -0.026^{+0.036}_{-0.053}$ (Planck + WL + BAO). In fact, when lensing is added to those data, it is found that the strength of the interaction decreases for the vacuum interaction scenario (see Table I of [81] for the details). In the current analysis for w_x varying in the interval $[-2, 0]$, we obtain similar results to those obtained in [30,80,81]. But, indeed, the results should not exactly match those in Refs. [30,80,81] since the astronomical data do not exactly match ours. Next we considered the interaction $Q \propto \rho_c\rho_x/(\rho_c + \rho_x)$ constrained in [62] for $w_x > -1$, and the interaction was found to be stable on large scales provided the coupling parameter was positive. The analysis [62] found that this nonzero coupling in the dark sector is favored with $\xi = 0.178^{+0.081}_{-0.097}$ at 1σ confidence level (Planck + WMAP9 + BAO + SNIa + H_0). The estimation of the coupling parameter in [62] is slightly greater than our estimate for $w_x \in [-2, 0]$. However, we note that the astronomical data in [62] and in the current work do not match exactly; thus, the differences may simply be due to the slightly different astronomical data under consideration. Finally, it might be interesting to make a detailed comparison with the well-known, stable, interacting, dark-energy models using the same astronomical data.

ACKNOWLEDGMENTS

The authors thank the referees for important comments. The use of the Markov chain Monte Carlo package CosmoMC in the analysis of the models is gratefully acknowledged by the authors. The work of W. Y. is supported by the National Natural Science Foundation of China under Grants No. 11705079 and No. 11647153. S. P. was supported by the SERB-NPDF programme (File No. PDF/2015/000640). J. D. B. was supported by the Science and Technology Facilities Council of the UK (STFC).

[1] P. A. R. Ade, N. Aghanim, M. Arnaud *et al.* (Planck Collaboration), Astron. Astrophys. **594**, A13 (2016).
[2] Y. Sofue and V. Rubin, Annu. Rev. Astron. Astrophys. **39**, 137 (2001).
[3] E. J. Copeland, M. Sami, and S. Tsujikawa, Int. J. Mod. Phys. D **15**, 1753 (2006).
[4] L. Amendola and S. Tsujikawa, *Dark Energy: Theory and Observations*, (Cambridge, Cambridge, England, 2010).
[5] C. Wetterich, Nucl. Phys. **B302**, 668 (1988).
[6] C. Wetterich, Astron. Astrophys. **301**, 321 (1995).
[7] S. Z. W. Lip, Phys. Rev. D **83**, 023528 (2011).
[8] P. J. E. Peebles, AIP Conf. Proc. **1241**, 175 (2010).
[9] L. Amendola, Phys. Rev. D **62**, 043511 (2000).
[10] L. Amendola, Mon. Not. R. Astron. Soc. **312**, 521 (2000).
[11] A. P. Billyard and A. A. Coley, Phys. Rev. D **61**, 083503 (2000).
[12] W. Zimdahl and D. Pavon, Phys. Lett. B **521**, 133 (2001).
[13] G. Olivares, F. Atrio-Barandela, and D. Pavón, Phys. Rev. D **71**, 063523 (2005).
[14] C. G. Bohmer, G. Caldera-Cabral, R. Lazkoz, and R. Maartens, Phys. Rev. D **78**, 023505 (2008).
[15] J.-H. He and B. Wang, J. Cosmol. Astropart. Phys. 06 (2008) 010.
[16] M. Quartin, M. O. Calvao, S. E. Joras, R. R. R. Reis, and I. Waga, J. Cosmol. Astropart. Phys. 05 (2008) 007.
[17] L. P. Chimento, Phys. Rev. D **81**, 043525 (2010).
[18] V. Salvatelli, N. Said, M. Bruni, A. Melchiorri, and D. Wands, Phys. Rev. Lett. **113**, 181301 (2014).
[19] S. Pan, S. Bhattacharya, and S. Chakraborty, Mon. Not. R. Astron. Soc. **452**, 3038 (2015).
[20] R. C. Nunes, S. Pan, and E. N. Saridakis, Phys. Rev. D **94**, 023508 (2016).
[21] S. Kumar and R. C. Nunes, Phys. Rev. D **94**, 123511 (2016).
[22] R. J. F. Marcondes, R. C. G. Landim, A. A. Costa, B. Wang, and E. Abdalla, J. Cosmol. Astropart. Phys. 12 (2016) 009.

[23] S. Pan and G. S. Sharov, Mon. Not. R. Astron. Soc. **472**, 4736 (2017).
[24] A. Mukherjee and N. Banerjee, Classical Quantum Gravity **34**, 035016 (2017).
[25] G. S. Sharov, S. Bhattacharya, S. Pan, R. C. Nunes, and S. Chakraborty, Mon. Not. R. Astron. Soc. **466**, 3497 (2017).
[26] W. Yang, N. Banerjee, and S. Pan, Phys. Rev. D **95**, 123527 (2017).
[27] J. Valiviita, E. Majerotto, and R. Maartens, J. Cosmol. Astropart. Phys. 07 (2008) 020.
[28] E. Majerotto, J. Valiviita, and R. Maartens, Mon. Not. R. Astron. Soc. **402**, 2344 (2010).
[29] T. Clemson, K. Koyama, G.-B. Zhao, R. Maartens, and J. Valiviita, Phys. Rev. D **85**, 043007 (2012).
[30] W. Yang and L. Xu, Phys. Rev. D **89**, 083517 (2014).
[31] W. Yang and L. Xu, J. Cosmol. Astropart. Phys. 08 (2014) 034.
[32] W. Yang and L. Xu, Phys. Rev. D **90**, 083532 (2014).
[33] W. Yang, H. Li, Y. Wu, and J. Lu, J. Cosmol. Astropart. Phys. 10 (2016) 007.
[34] R. F. vom Marttens, L. Casarini, W. S. Hipólito-Ricaldi, and W. Zimdahl, J. Cosmol. Astropart. Phys. 01 (2017) 050.
[35] R. G. Cai, N. Tamanini, and T. Yang, J. Cosmol. Astropart. Phys. 05 (2017) 031.
[36] J. D. Barrow and T. Clifton, Phys. Rev. D **73**, 103520 (2006).
[37] N. Kaiser, Mon. Not. R. Astron. Soc. **227**, 1 (1987).
[38] A. J. S. Hamilton, Astrophys. Space Sci. Lib. **231**, 185 (1998).
[39] L. Samushia, W. J. Percival, and A. Raccanelli, Mon. Not. R. Astron. Soc. **420**, 2102 (2012).
[40] Y.-S. Song and W. J. Percival, J. Cosmol. Astropart. Phys. 10 (2009) 004.
[41] M. Bartelmann and P. Schneider, Phys. Rep. **340**, 291 (2001).
[42] C. Heymans *et al.*, Mon. Not. R. Astron. Soc. **432**, 2433 (2013).
[43] M. Asgari, C. Heymans, C. Blake, J. Harnois-Deraps, P. Schneider, and L. V. Waerbeke, Mon. Not. R. Astron. Soc. **464**, 1676 (2017).
[44] L. Xu, Phys. Rev. D **87**, 043525 (2013).
[45] L. Xu, Phys. Rev. D **88**, 084032 (2013).
[46] L. Xu, J. Cosmol. Astropart. Phys. 02 (2014) 048.
[47] W. Yang, L. Xu, Y. Wang, and Y. Wu, Phys. Rev. D **89**, 043511 (2014).
[48] B. Chang and L. Xu, Phys. Rev. D **90**, 027301 (2014).
[49] B. Chang, J. Lu, and L. Xu, Phys. Rev. D **90**, 103528 (2014).
[50] L. Xu, Phys. Rev. D **91**, 063008 (2015).
[51] L. Xu, Phys. Rev. D **91**, 103520 (2015).
[52] Y. Chen and L. Xu, Phys. Lett. B **752**, 66 (2016).
[53] H. Zhang, E. Li, and L. Xu, arXiv:1605.00213.
[54] C. P. Ma and E. Bertschinger, Astrophys. J. **455**, 7 (1995).
[55] V. F. Mukhanov, H. A. Feldman, and R. H. Brandenberger, Phys. Rep. **215**, 203 (1992).
[56] K. A. Malik and D. Wands, Phys. Rep. **475**, 1 (2009).
[57] K. Koyama, R. Maartens, and Y.-S. Song, J. Cosmol. Astropart. Phys. 10 (2009) 017.
[58] W. Hu, Astrophys. J. **506**, 485 (1998).
[59] H. Kodama and M. Sasaki, Prog. Theor. Phys. **78**, 1 (1984).
[60] M. B. Gavela, D. Hernandez, L. Lopez Honorez, O. Mena, and S. Rigolin, J. Cosmol. Astropart. Phys. 07 (2009) 034.
[61] M. B. Gavela, L. Lopez Honorez, O. Mena, and S. Rigolin, J. Cosmol. Astropart. Phys. 11 (2010) 044.
[62] Y. H. Li and X. Zhang, Phys. Rev. D **89**, 083009 (2014).
[63] M. Chevallier and D. Polarski, Int. J. Mod. Phys. D **10**, 213 (2001).
[64] E. V. Linder, Phys. Rev. Lett. **90**, 091301 (2003).
[65] R. Adam, P. A. R. Ade, N. Aghanim *et al.* (Planck Collaboration), Astron. Astrophys. **594**, A1 (2016).
[66] N. Aghanim, M. Arnaud, M. Ashdown *et al.* (Planck Collaboration), Astron. Astrophys. **594**, A11 (2016).
[67] M. Betoule *et al.* (SDSS Collaboration), Astron. Astrophys. **568**, A22 (2014).
[68] F. Beutler, C. Blake, M. Colless, D. Heath Jones, L. Staveley-Smith, L. Campbell, Q. Parker, W. Saunders, and F. Watson, Mon. Not. R. Astron. Soc. **416**, 3017 (2011).
[69] A. J. Ross, L. Samushia, C. Howlett, W. J. Percival, A. Burden, and M. Manera, Mon. Not. R. Astron. Soc. **449**, 835 (2015).
[70] H. Gil-Marín *et al.*, Mon. Not. R. Astron. Soc. **460**, 4210 (2016).
[71] H. Gil-Marín *et al.*, Mon. Not. Roy. Astron. Soc. **465**, 1757 (2017).
[72] C. Heymans *et al.*, Mon. Not. R. Astron. Soc. **432**, 2433 (2013).
[73] M. Asgari, C. Heymans, C. Blake, J. Harnois-Deraps, P. Schneider, and L. Van Waerbeke, Mon. Not. R. Astron. Soc. **464**, 1676 (2017).
[74] M. Moresco, L. Pozzetti, A. Cimatti, R. Jimenez, C. Maraston, L. Verde, D. Thomas, A. Citro, R. Tojeiro, and D. Wilkinson, J. Cosmol. Astropart. Phys. 05 (2016) 014.
[75] A. G. Riess *et al.*, Astrophys. J. **826**, 56 (2016).
[76] J. D. Barrow, Phys. Rev. D **89**, 064022 (2014).
[77] A. Lewis, A. Challinor, and A. Lasenby, Astrophys. J. **538**, 473 (2000).
[78] A. Lewis and S. Bridle, Phys. Rev. D **66**, 103511 (2002).
[79] S. Kumar and R. C. Nunes, Phys. Rev. D **96**, 103511 (2017).
[80] E. Di Valentino, A. Melchiorri, and O. Mena, Phys. Rev. D **96**, 043503 (2017).
[81] Y. H. Li, J. F. Zhang, and X. Zhang, Phys. Rev. D **93**, 023002 (2016).